

T-2043

PLANE WAVES IN AN ELASTICALLY
ANISOTROPIC MEDIUM

by

Jeffrey H. Copley

ProQuest Number: 11016458

All rights reserved

INFORMATION TO ALL USERS

The quality of this reproduction is dependent upon the quality of the copy submitted.

In the unlikely event that the author did not send a complete manuscript and there are missing pages, these will be noted. Also, if material had to be removed, a note will indicate the deletion.



ProQuest 11016458

Published by ProQuest LLC (2019). Copyright of the Dissertation is held by the Author.

All rights reserved.

This work is protected against unauthorized copying under Title 17, United States Code
Microform Edition © ProQuest LLC.

ProQuest LLC.
789 East Eisenhower Parkway
P.O. Box 1346
Ann Arbor, MI 48106 – 1346

A thesis submitted to the Faculty and the Board of Trustees of the Colorado School of Mines in partial fulfillment of the requirements for the degree of Master of Science, Geophysics.

Signed: Jeffrey H. Copley
Jeffrey H. Copley

Golden, Colorado

Date: March 20, 1978

Approved: J. E. White
J. E. White
Thesis Advisor

Golden, Colorado

Date: MARCH 23, 1978

Approved: G. V. Keller
George V. Keller
Head of Department of
Geophysics

Golden, Colorado

Date: March 23, 1978

ABSTRACT

Knowledge of wave propagation in elastically anisotropic materials has long been a topic of interest. A system of particles, called cuboids, is developed in which elastic constants (compressional and shear) can be theoretically calculated as a function of stress in three mutually orthogonal directions. These stress dependent elastic constants are then used in the solution of the wave equation. This results in three solutions for velocity and particle motion, which correspond to three body phases of propagation, in any arbitrary direction through this anisotropic medium. As this is done for many arbitrary directions, the spatial variation of velocity and particle motion is defined for each phase of propagation.

The spatial variation of the body wave velocity in elastically anisotropic materials can be 10% or more. The magnitude of this change in velocity with direction is found to be primarily affected by the relative magnitude of the shear modulus. Materials which show low V_s/V_p ratios can be expected to show large (greater than 10%) spatial changes in velocity.

Particle motion of the three body waves P, SH, and SV can be described as longitudinal, transverse-horizontal, and transverse-vertical, respectively. In materials showing elastic anisotropy these vibration directions are skewed as much as $5 - 10^\circ$ from the assumed vibration for compressional waves and as much as 45° for the transverse waves.

The results of this paper can be summarized briefly in the following conclusions:

- The spatial variation of both the compressional and shear velocity is large enough (5 - 10%) to be seen with modern recording equipment.
- The magnitude of the velocity variation is dependent on the relative value of the shear modulus.
- If the velocity and particle motion of the compressional and shear waves are known, the relative magnitude and orientation of the stresses can be determined.
- The particle motion of the plane wave does not correspond to that of the conventional far-field seismic modes of propagation (P, SH, SV).

TABLE OF CONTENTS

	Page
Abstract	iii
List of Illustrations	vi
Acknowledgments	vii
Introduction	1
Scope of Work	1
Background	3
Theory	10
The Model	10
The Elasticity of the Cuboid Packing	16
Solution of the Wave Equation	25
Results	34
Case I	38
Case II	46
Discussion	53
Spatial Variation of Velocity	53
Spatial Variation of Particle Motion	55
Experimental Elastic Anisotropy	61
Conclusions	68
Appendix	71
A: Solution of the Wave Equation	71
B: Derivation of the Undeformed Porosity	74
Selected References	76

LIST OF ILLUSTRATIONS

	Page
1. Cuboid and simple cubic packing	4
2. Geometry of cuboids in contact	11
3. Compressional wave propagation in uniaxially loaded rock cores (after Benzing, 1973)	14
4. Porosity of cuboid packing	17
5. Velocity vs. depth in packing	21
6. Contact subjected to incremental shear stress	22
7. Coordinate axes and associated elastic constants	26
8. Geometry of propagation	32
9. Velocity vs. propagation direction (Case I)	41
10. Particle motion. Case I = 0	42
11. Particle motion. Case I = 15	43
12. Particle motion. Case I = 30	44
13. Particle motion. Case I = 45	45
14. Velocity vs. propagation direction (Case II)	48
15. Particle motion. Case II = 0	49
16. Particle motion. Case II = 15	50
17. Particle motion. Case II = 30	51
18. Particle motion. Case II = 45	52
19. Velocity vs. propagation direction	56
20. Particle motion for compressional wave in an anisotropic medium	58
21. Experimental results. (After Nur and Simmons, 1969)	65

Acknowledgements

I would like to thank my advisor, J. E. White, and my committee members P. R. Romig, F. R. Yeatts, and M. W. Major, for their help in the completion of this thesis. Special thanks goes to Dick Yeatts, whose continued insights and patience aided considerably in the solution of the many problems encountered in this work. Throughout my tenure at the Colorado School of Mines I have been financially supported by a fellowship from the Department of Health, Education, and Welfare; for this I am grateful.

The production of a thesis creates many trials and tribulations for its author. This thesis would never have reached fruition without the encouragement from my many good friends. John Arestad and Juan-Carlos Rodriguez deserved special thanks for numerous discussions and cups of coffee. My fondest thoughts are for Julie, who kept both reality and my sanity within my grasp through many difficult times.

INTRODUCTION

Scope of Work

During the last fifteen years attempts have been made to determine in situ stress levels in earth materials using seismic waves. Seismologists have obtained mixed results studying V_s/V_p ratios as indicators of present or changing stress levels. For the most part these studies have been related to earthquake precursor phenomena and the like. Their work in general does not consider the spatial variation in velocity, but rather the change in velocity, with respect to time in one or two directions.

This paper offers a theoretical explanation of the spatial variation of velocity and particle motion as observed in an elastically anisotropic material. This can be related to anisotropic stress systems by assuming that the elastic anisotropy is due to stress. It is found that relative stress levels can be determined along with their orientation if detailed examination is made of all body phases of propagation. Some of the effects which are crucial in the determination of the stress system are

T-2043

subtle and may not be observable with conventional instrumentation. The method and ideas presented offer an alternative interpretation to existing data and suggest phenomena which might hold the key to determining in situ stress levels.

Background

Detailed knowledge of the velocity and particle motion of a seismic wave may lead to a determination of the stress environment. From the results presented here it is seen that this may indeed be possible. A theoretical model of a porous material is used to calculate the necessary elastic constants. These elastic constants are then used in the solution of the homogeneous wave equation. Solutions of this equation define the velocity and particle motion of a plane wave traveling in an arbitrary direction.

The elementary particle of the model is called a cuboid. A cuboid is a cube with spherical caps on each face. Figure 1-b is a side view of a cuboid. These particles are assembled in a simple cubic packing as shown in Figure 1-a. As shown in the figure, this type of packing has three orthogonal axes, each of which is oriented normal to a face of a cube.

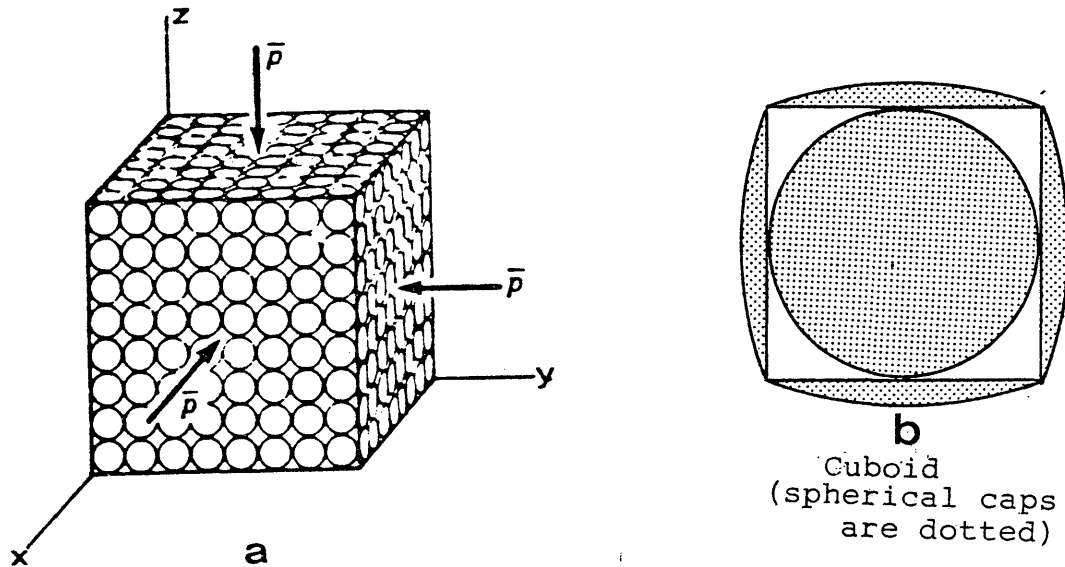


Figure 1
Cubic packing and Cuboid
(with caps dotted)

It can be seen that if the radius of the spherical cap were changed, the porosity of the packing would also change. Previous models of porous materials utilized packings of spheres. White (1965), Gassman (1951) and others used packings (simple cubic, hexagonal, etc.) of uniformly sized spheres. Brandt (1955) used a very complicated packing of randomly sized spheres to approximate

low porosity materials. In the packings of uniform spheres the relation for stress and strain are simple but the porosity must remain fixed. In the packing of randomly sized spheres the porosity is low but all mathematical descriptions are complicated. The prime advantage of the cuboid model is the mathematical simplicity of uniform curvature at the contacts and a porosity which can be selected over a wide range.

The fundamental equations in the development of this thesis are those which describe the behavior of two identical spheres in contact. These relations were derived by Hertz (1881). A good discussion of Hertz's theory can be found in White (1965) and Love (1944). If the assumption is made that all the deformation takes place in the neighborhood of the contact, then these equations can be used to describe two cuboids in contact at a spherical cap. Gassman (1951) considered a hexagonal packing of uniform spheres and determined the velocity and ray paths of an elastic plane wave traveling only vertically or horizontally. In his derivation of compressional and shear elastic constants he neglects the effects of the tangential forces produced at

the contacts between spheres. This leaves the development of his work somewhat incomplete. Mindlin (1949) developed relations for the tangential compliance of uniform spheres in contact. In a later paper Mindlin and his co-workers (1951) continued the investigation into tangential forces and how attenuation occurs. This work led to conclusions that when two spheres are in contact and subjected to a tangential force, slip takes place in an annulus around the area of contact. White (1966) carried this line of thinking further by proposing that this slip is one of the main sources of attenuation in the propagation of a seismic wave.

White (1953) has published work relating to velocity as a function of stress in a simple cubic packing of spheres. In this paper he uses Hertz's relations to develop expressions for the axial elastic constants (compressional and shear) in the sphere pack. These relations show good qualitative agreement with experimental results for velocities in near surface formations. In a later paper (White, 1964) he again uses the simple cubic packing of spheres, but this time presents some relations

for the two dimensional variations of compressional and shear velocity, which he concludes to be of a negligible amount. From the work of these authors certain conclusions can be summarized, which are also examined in this thesis:

- 1) velocity should be approximately proportional to the sixth root of pressure,
- 2) velocity is relatively constant with respect to azimuth in a simple cubic packing of spheres,
- 3) a qualitative comparison between sphere pack models and experimental data for various granular media, shows good agreement (White, et al, 1953, Brandt, 1955).

Out of necessity this thesis is of a limited scope. The cuboid packing was considered to be without pore fluids. Arbitrary stresses were applied only in the axial direction in two configurations. In Case I the three axial stresses were set equal to a value of arbitrary magnitude ($\sigma_x = \sigma_y = \sigma_z = 11.9$ bars). Case II had the stresses in the x and y directions 20% less than that in

T-2043

the z direction ($\sigma_x = \sigma_y = 9.52$ bars, $\sigma_z = 11.9$ bars). The curvature of all of the spherical caps was the same. A plane sinusoidal elastic wave of arbitrary frequency (wavelength assumed long with respect to the cuboid) was used in the solution of the wave equation. Since the results are independent of frequency (in the low frequency range), the expressions apply directly to transient waveforms as well. Attenuation was not considered.

The results of this thesis can be summarized briefly in the following conclusions:

- The spatial variation of both the compressional and shear velocity is large enough (5 - 10%) to be seen with modern recording equipment, under favorable conditions.
- The magnitude of the velocity variation is dependent on the relative value of the shear modulus.
- If the velocity and particle motion of the compressional and shear waves are known, the relative magnitude and orientation of the stresses can be determined.

- The particle motion of the plane wave does not correspond to that of the conventional far field seismic modes of propagation (P, SH, SV).

THEORY

In this section the necessary relations are developed to describe the elastic behavior and are applied to the solution of the wave equation. A presentation is also made of the method of solution of the wave equation.

The Model

A simple cubic packing of cuboid particles is used to develop relations between stress and strain. These elastic constants are then used in the homogeneous wave equation in order to find solutions corresponding to the velocity and particle motion for plane waves. There are two distinct advantages to the cuboid model: First, at the contact, there are two spherical surfaces in contact. This allows the retention of the relations developed for two spheres in contact. Secondly, since the radius of the cap is arbitrary, the porosity and elastic moduli can be readily modified without complicating any of the relations. These changes cannot be made in the conventional sphere pack without complicating all relations.

Figure 2 illustrates the geometry of a general contact. Two cuboids, of cap radius A , are compressed by an axial force G distributed across the face of the unit cube. Due

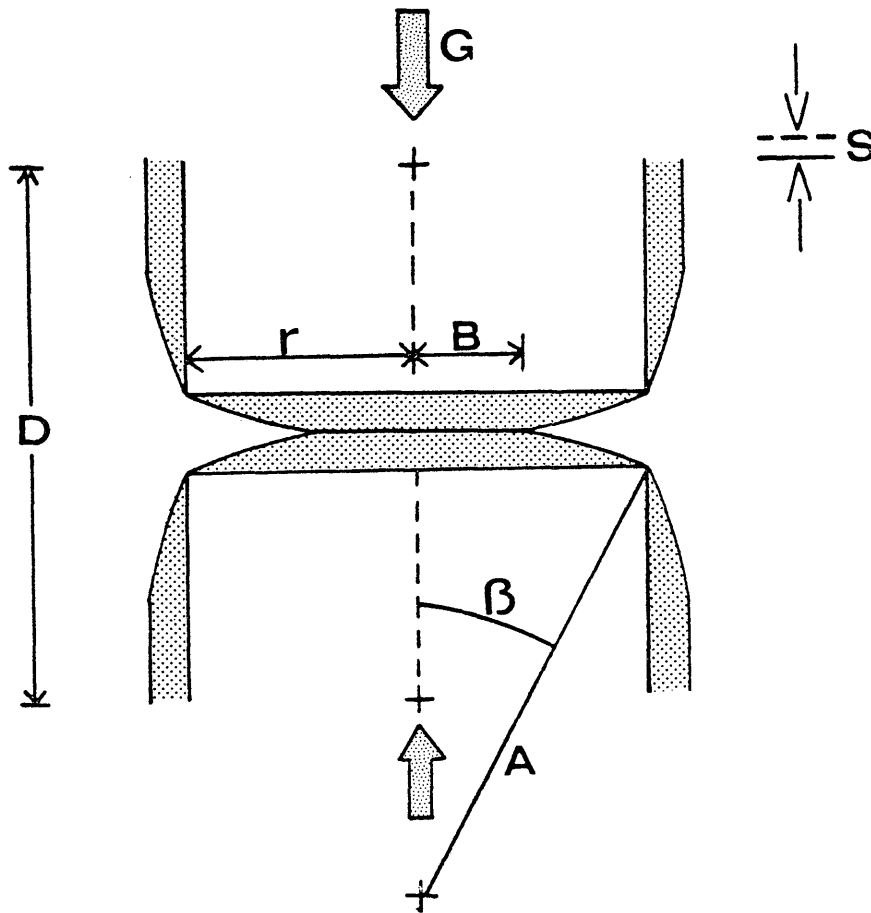


Figure 2
Geometry of Cuboids in Contact

T-2043

to the application of this axial force, the centers of the two cuboids approach one another by a distance S (White, 1965):

$$S = \left\{ 9(1 - \nu^2)^2 \frac{G^2}{2E^2A} \right\}^{1/3} \quad (1)$$

where E is Young's modulus and ν is Poisson's ratio. The two surfaces come into contact over a circular area of radius B :

$$B = \left(3(1 - \nu^2) \frac{AG}{4E} \right)^{1/3} \quad (2)$$

Before these equations can be applied to the cuboid model, an assumption must be made. This can be stated as follows:

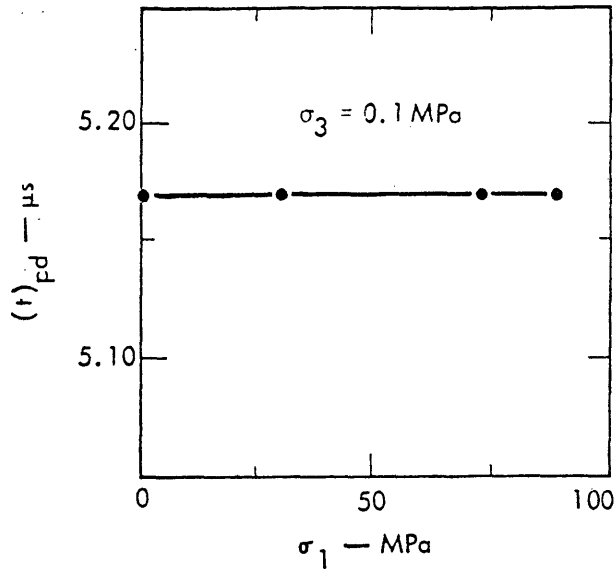
- All significant deformation is confined to a volume, around the contact, which is small compared to the volume of the cuboid.

In other words stresses in one axial direction do not influence stresses in the transverse directions. This can also be stated as the stress in one axial direction has no

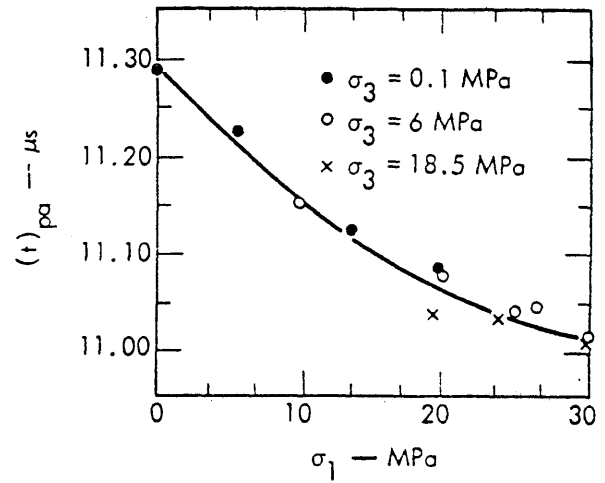
T-2043

effect on the compressional velocity in the transverse directions.

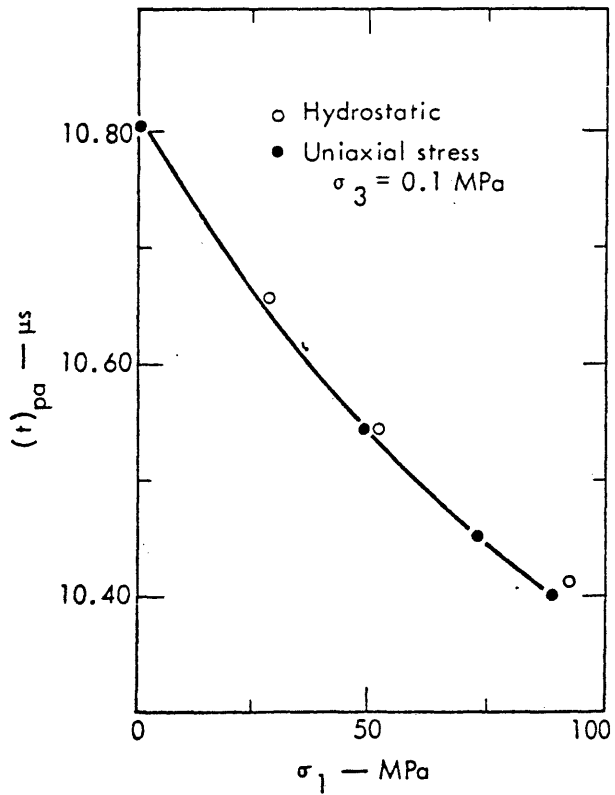
This assumption can be supported by some experimental work (Benzing, et al, 1973). Figure 3 is taken from Benzing (1973) and shows the results of his work with compressional waves in rock cores. Cylindrical cores were cut from granodiorite samples and subjected to various values of axial stress (σ_1) and confining stress (σ_3). Compressional waves were then propagated in either the axial or diametral directions, with travel time being recorded. In Figure 3-a the compressional wave was propagated in the diametral direction, at a constant confining pressure, with increasing axial stress. Over the range of stresses, well within the elastic range, there is no measurable change in the travel time. In Figure 3-b the compressional wave is propagated in the axial direction at a constant confining pressure and increasing axial stress. For this case the travel time decreases (or velocity increases) a large amount. This figure also shows that it makes little difference if the stresses are hydrostatic ($\sigma_1 = \sigma_3$) or uniaxial ($\sigma_1 \gg \sigma_3$). Figures C and D show the same effects



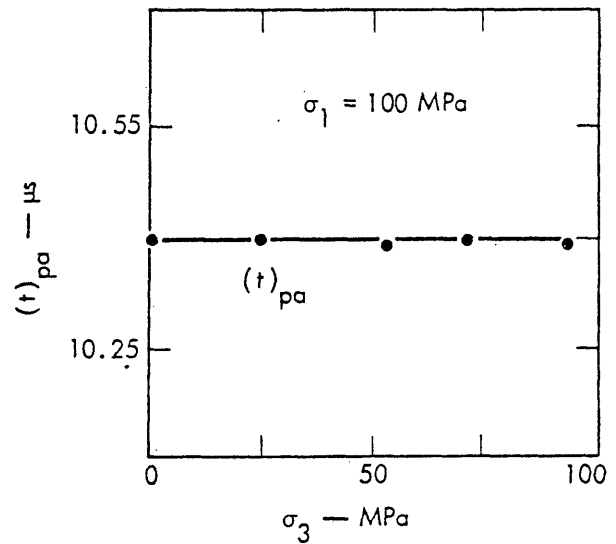
a Compressional wave travel time in the diametral direction vs axial stress.



c Compressional wave travel time in the axial direction vs axial stress at various confining pressures.



b Compressional wave travel time in the axial direction vs axial stress.



d Compressional wave travel time in the axial direction vs confining pressure (σ_1 constant).

Figure 3

Compressional wave propagation in uniaxially loaded rock cores. (1MPa = 10bars)

(after Benzing, et al, 1973)

T-2043

for other combinations of propagation direction and stress direction. Taken together these results support the assumption that velocity is unaffected by stresses oriented normal to the direction of propagation, provided that the stresses remain within the elastic limits of the material.

A restriction imposed on this model is that the stresses remain within the elastic region. This requires some arbitrary failure criterion to determine when a stress is too great. The maximum stress allowed for any value of A will be that which produces radius of contact greater than one-tenth the size of the cap. In other words, when B becomes greater than one-tenth r (one-half the length of the cuboid edge) the model is arbitrarily assumed to have reached the elastic limit.

From the geometry of the contact area, Figure 2, and that of the cuboid particle, it is not difficult to calculate the porosity of an unstressed packing as a function of the cap radius A. The derivation appears in Appendix B and the result is shown in equation (3):

$$\text{Porosity} = 1 - \frac{\pi A^3 \left[2 - \cos\beta (2 + \sin^2\beta) \right] + 4r^3}{4(r + A(1 - \cos\beta))^3} \quad (3)$$

T-2043

This equation is presented graphically in Figure 4. A maximum porosity of 67% is obtained when $A/r = 1$. At $A/r = 100$ the void space is about 1% of the total volume. As the cuboid pack undergoes loading and is compacted, the porosity is slightly reduced. The total change in porosity at the failure criterion for any value of A/r , amounts to less than 10% of the initial value. This means that the bulk density will increase by a small amount at low porosity. Since the velocity is inversely proportional to the square root of the bulk density, this effect will not be significant.

The Elasticity of the Cuboid Packing

The compressional elastic constant is written as the ratio of incremental normal stress to incremental strain. White (1965) presents the relation between incremental force and incremental displacement for two spheres in contact as,

$$\frac{\Delta G}{\Delta S} = \left(\frac{3AE^2G}{4(1 - \nu^2)^2} \right)^{1/3} \quad (4)$$

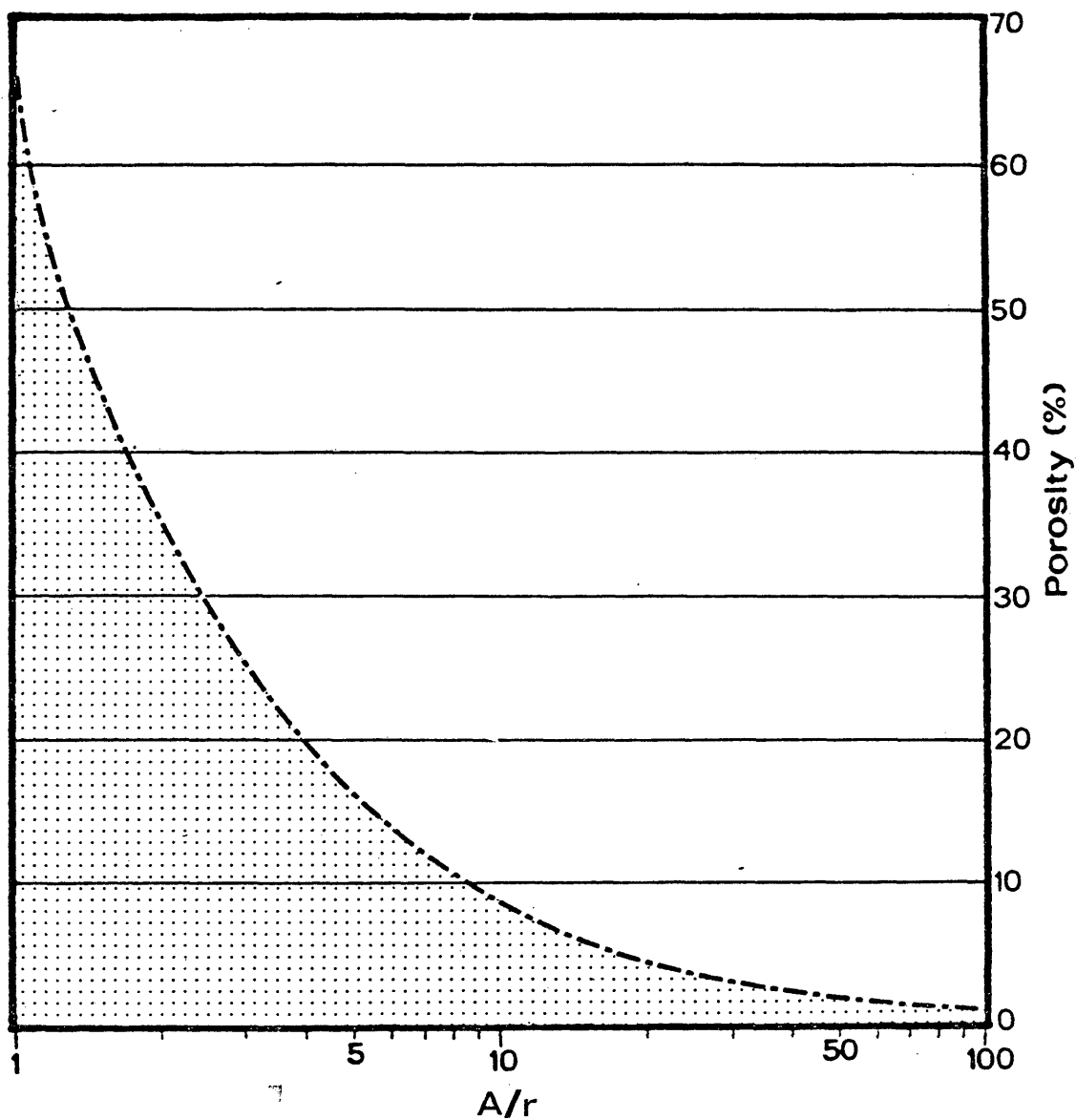


Figure 4

The porosity of a simple cubic packing of cuboids is shown as a function of A/r . The packing is unstressed and is the maximum possible porosity. When the pack is stressed the porosity will decrease about 10% (of the initial value), at the highest stress applied.

T-2043

where G is the preloading normal force. Through the previous assumption this equation for two spheres can also be used for two cuboids in contact. The additional normal force, ΔG , is assumed to be distributed evenly over the face of the unit cube yielding an average stress $\overline{\Delta p}$, of,

$$\overline{\Delta p} = \frac{\Delta G}{D_y D_z} \quad (5)$$

where D is the distance between the centers of two cuboids along the appropriate axis and is written as,

$$D = 2\{r + A(1 - \cos\beta) - S/2\} \quad (5a)$$

The additional displacement, ΔS , due to the incremental force ΔG can be written as an average strain $\overline{\Delta \epsilon}$

$$\overline{\Delta \epsilon} = \frac{\Delta S}{D_x} \quad (6)$$

The compressional elastic constant in an axial direction, for the cuboid array is written as,

T-2043

$$K_p = \frac{\overline{\Delta P}}{\Delta \epsilon}$$

Realizing that in this model the differences between D_x , D_y and D_z are insignificant, equations 4, 5 and 6 can be combined to express the axial compressional elastic constant as,

$$K_p = \frac{1}{D} \left(\frac{3AE^2G}{4(1-\nu^2)^2} \right)^{1/3} \quad (7)$$

wherein ν is the Poisson's ratio of the material of which the cuboid is composed. From this expression (7) the compressional velocity can be written as,

$$v_p = \left\{ \frac{K_p}{\bar{\rho}} \right\}^{1/2}$$

where $\bar{\rho}$, the average density is written as $\bar{\rho} = (1 - \phi)\rho_s$ (ϕ is the porosity and ρ_s is the density of the cuboid material).

In Figure 5 the velocity is plotted as a function of depth in a gravity loaded simple cubic packing of cuboids, for various values of A/r . Depth was plotted instead of

T-2043

stress, because for any value of cap radius the bulk density is different. Hence, the preloading force, G , is a different function of depth. This preloading force, G , can be written as a function of depth as,

$$G = (\bar{\rho} g z D^2)$$

where z is depth and g is the acceleration of gravity. The velocity can now be written as a function of depth in the form,

$$v_p = \left\{ \frac{1}{\rho} \left(\frac{3AE^2}{4(1 - \nu^2)^2} (\rho g \frac{z}{D}) \right)^{1/3} \right\}^{1/2}$$

The dotted curve labeled, W , is the velocity-depth relation calculated by White (1965) for a gravity loaded simple cubic packing of spheres. The results for the sphere pack can be directly compared with a simple cubic packing of cuboids of $A/r = 1$. In making this comparison it is found that the cuboids velocity should be 1.05 of the dashed curve for the sphere pack velocity.

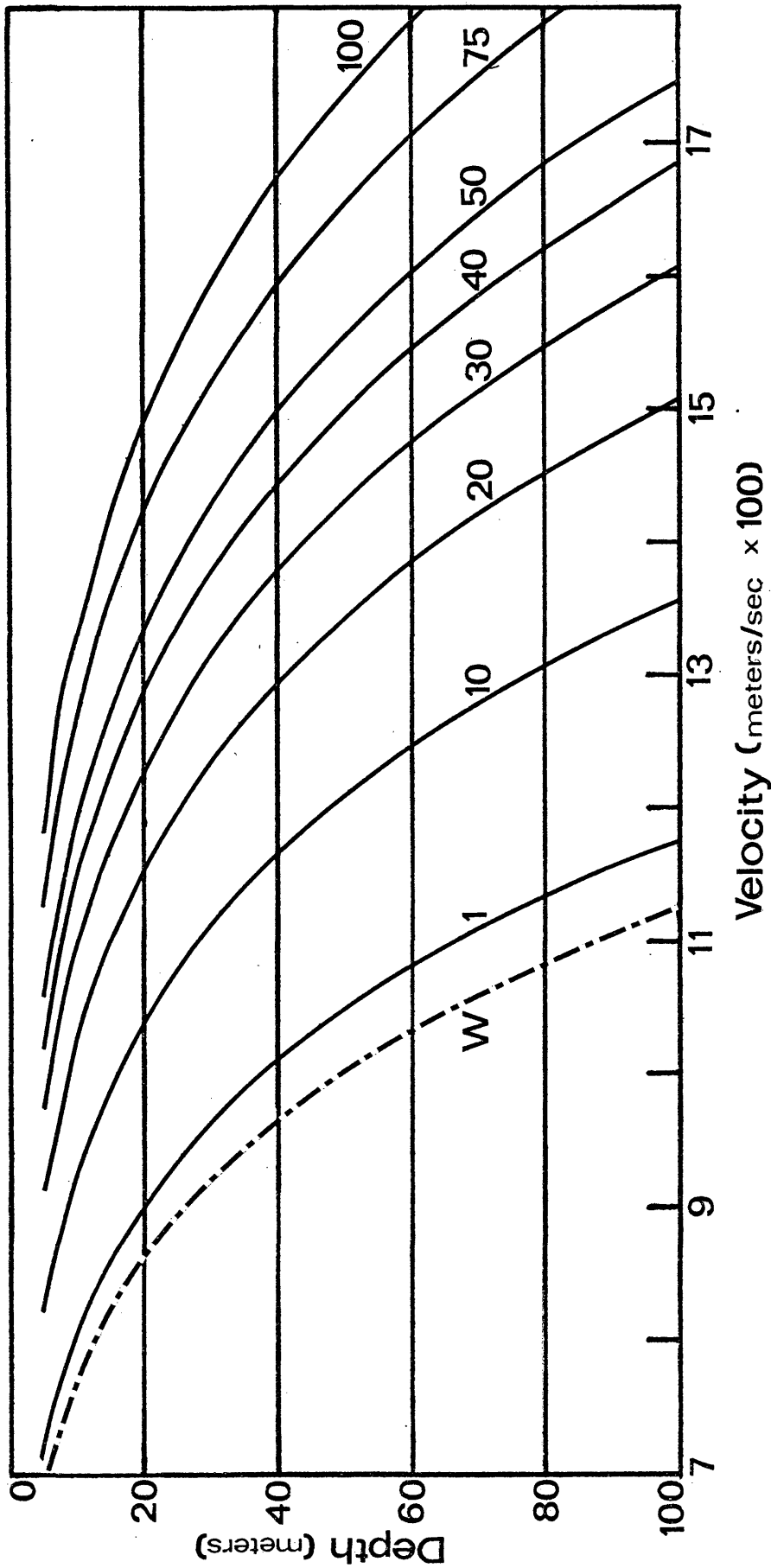


Figure 5

The axial compressional velocity is shown as a function of axial stress, or depth. In this model the pack is assumed to be loaded with gravity. Values of A/r appear adjacent to the curves. The dotted curve, W , has been calculated for a sphere pack by White (1965).

of the shear elastic constant proceeds
of argument. Figure 6 shows some

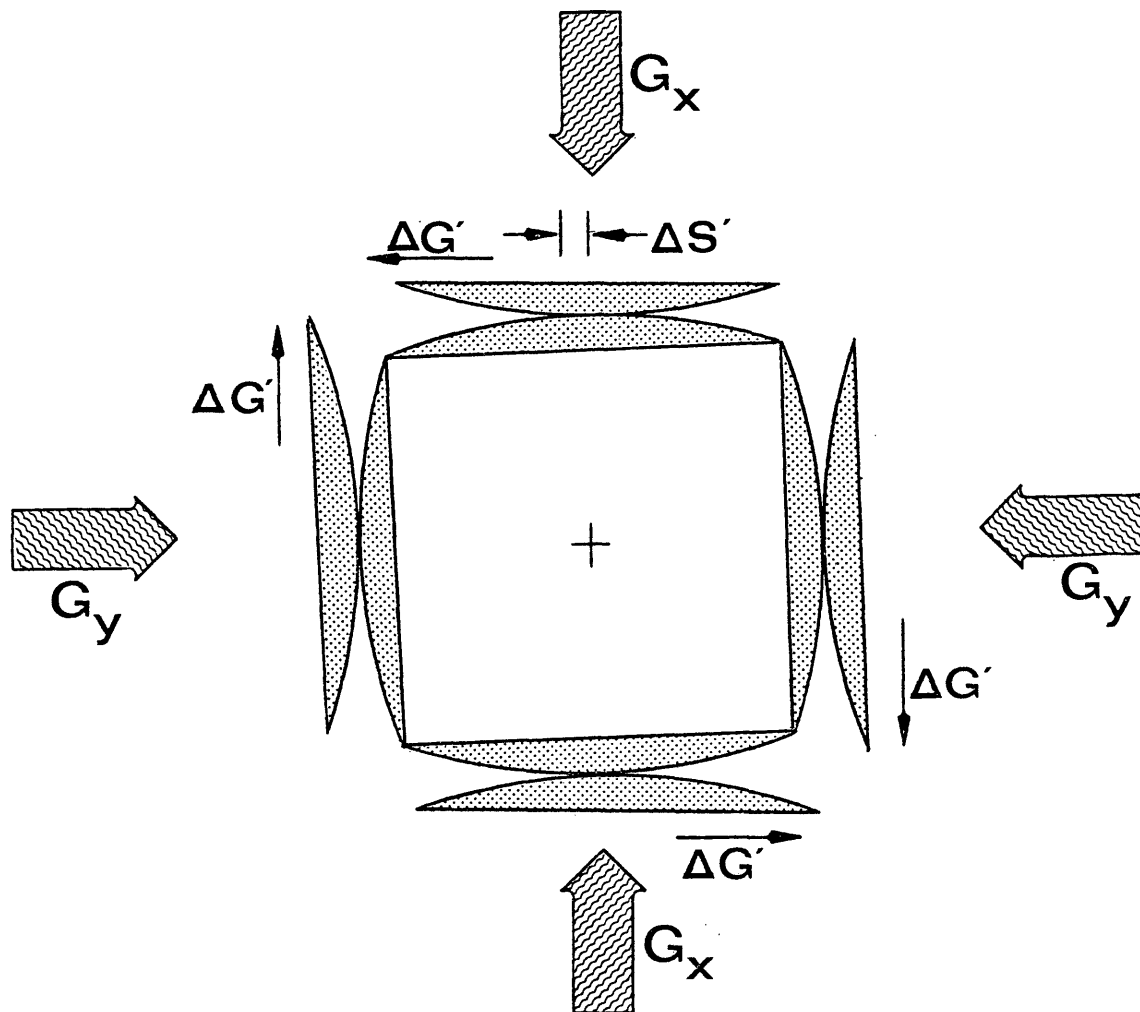


Figure 6

etry of cuboids in contact
r shearing force.

For a simple cubic packing of spheres, the relation between incremental values of shear force $\Delta G'$ and incremental shear displacement, $\Delta S'$, is given by White (1965) as,

$$\frac{\Delta G'}{\Delta S'} = \frac{(6(1 - \nu^2) AE^2 G)^{1/3}}{(2 - \nu)(1 + \nu)} \quad (8)$$

where G is the normal preloading force. In the sphere pack (Figure 1a) two equal and opposite incremental shear forces, of magnitude $\Delta G'$, cause the spheres to rotate until a compensating torque is provided by horizontally adjacent spheres. Each of these four forces has a magnitude of $\Delta G'$. This argument is applied to the cuboid model by assuming that all significant deformation takes place in a small volume around the contact. In addition, the cuboid model does not require the axial preloading forces to be equal.

As in the sphere pack, an incremental shear force exists across each contact and the resulting shear displacement across the contact is dependent on the preloading force normal to the contact. In Figure 6 a force, $\Delta G'$, oriented in the y direction is applied across the contacts

T-2043

normal to the x direction. A displacement of $\Delta S'_x$ occurs at these contacts and $\Delta S'_y$ is produced across the contacts normal to the y direction. These displacements are unequal because the axial preloading forces G'_x and G'_y are unequal. The total shear displacement is $\Delta S'$ and is,

$$\Delta S' = \Delta S'_x + \Delta S'_y \quad (9)$$

The average shear strain is then written as

$$\bar{\Delta \epsilon}_s = \frac{\Delta S'}{D_x} \quad (10)$$

The shear force $\Delta G'$ is distributed across the face of the unit cube. The average shear stress $\Delta \bar{p}_s$,

$$\Delta \bar{p}_s = \frac{\Delta G'}{D_y D_z} \quad (11)$$

The shear elastic constant for incremental shear stress in the axial direction is written as

$$K_s = \frac{\Delta \bar{p}_s}{\bar{\Delta \epsilon}_s} = \frac{1}{D} \frac{\Delta G'}{\Delta S'} = \frac{1}{D} \left(\frac{\Delta G'}{\Delta S'_x + \Delta S'_y} \right)$$

T-2043

Substituting the previous equations and simplifying the shear elastic constant becomes,

$$C_{66} = K_s = \frac{1}{D} \left(\frac{(6(1-\nu^2)AE^2)^{1/3}}{(2-\nu)(1+\nu)} \right) \left(\frac{1}{\left(\frac{1}{G_x} \right)^{1/3}} + \frac{1}{\left(\frac{1}{G_y} \right)^{1/3}} \right) \quad (12)$$

K_s in this case is the shear modulus C_{66} . The C_{44} and C_{55} moduli are found similarly. The speed of a transverse wave travelling along the x-axis with motion in the y-direction (or travelling in the y-direction with motion along the x-axis) is,

$$v_s = \left\{ \frac{K_s}{\rho} \right\}^{1/2}$$

In actual practice the difference between D_x , D_y and D_z is small enough to be discounted.

The Solution of the Wave Equation

In a simple cubic packing there are three orthogonal axes of orthotropic symmetry. These are the direction in which the forces are applied and the elastic constants are calculated. Figure 7 shows the three axes (x, y, and z)

T-2043

and the two elastic constants calculated for each direction (one compressional and one shear). These elastic coefficients are written as they appear in the equations. The C_{11} , C_{22} , C_{33} constants are compressional and the C_{44} , C_{55} , C_{66} values are the shear constants.

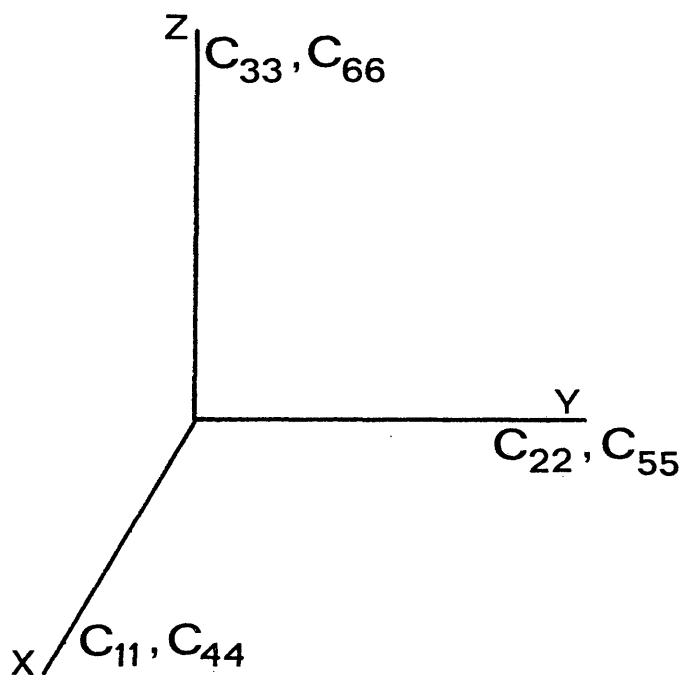


Figure 7
Coordinate axes and associated elastic constants.

T-2043

Now that the elastic constants have been defined the expressions for the propagation of a plane wave, through this model, will be derived.

The homogeneous wave equation can be written, for plane waves of small amplitude, as,

$$\rho \frac{\partial^2 U_i}{\partial t^2} = \frac{\partial \Psi_{ij}}{\partial x_j} \quad (12)$$

where U_i is the particle displacement along the i^{th} axis and Ψ_{ij} summation over repeated indices assumed can be written as,

$$\Psi_{ij} = \frac{\partial W}{\partial e_{ij}} \quad (12a)$$

and,

$$\begin{aligned} e_{ij} &= \frac{\partial U_i}{\partial x_j} ; i = j \\ &= \frac{\partial U_i}{\partial x_j} + \frac{\partial U_j}{\partial x_i} ; i \neq j \end{aligned}$$

where W is the strain energy density function. For this

T-2043

particular model this function is written as,

$$2W = C_{11}e_{11}^2 + C_{22}e_{22}^2 + C_{33}e_{33}^2 + 2(C_{12}e_{11}e_{22} + C_{13}e_{11}e_{33} + C_{23}e_{22}e_{33}) + C_{44}e_{23}^2 + C_{55}e_{31}^2 + C_{66}e_{12}^2$$

where the C_{ij} terms are the appropriate elastic constants and e_{ij} the strains. From the assumption which was made earlier, that stress changes along an axis do not affect stresses in the transverse directions, it can be stated that,

$$C_{12} = C_{23} = C_{13} = 0$$

$$\begin{aligned} P_{yz} &= C_{44} G_{yz} \\ P_{zx} &= C_{55} G_{zx} \\ P_{xy} &= C_{66} G_{xy} \end{aligned}$$

This simplifies the strain energy density function W to,

$$2W = C_{11}e_{11}^2 + C_{22}e_{22}^2 + C_{33}e_{33}^2 + C_{44}e_{23}^2 + C_{55}e_{31}^2 + C_{66}e_{12}^2 \quad (13)$$

The component of particle displacement on the j^{th} axis can be written as a time variant function of the form,

$$U_j = A_j \exp \{i n (\alpha_1 x_1 + \alpha_2 x_2 + \alpha_3 x_3 - vt)\};$$

$$j = 1, 2, 3 \quad (14)$$

where A_j is the amplitude of the particle motion on the j^{th} axis, i is the imaginary number $\sqrt{-1}$, n is an arbitrary wave number, $\alpha_{1, 2, 3}$ is the direction cosine between the direction of propagation and the $1, 2, 3^{\text{th}}$ axis, and v is the velocity of the plane wave.

Differentiating statement 14, with respect to time and space, results in terms of two types as shown below,

$$\frac{\partial^2 U_j}{\partial t^2} = -A_j n^2 v^2 \exp \{i n (\alpha_1 x_1 + \alpha_2 x_2 + \alpha_3 x_3 - vt)\}$$

and

$$\frac{\partial^2 U_j}{\partial x_k \partial x_m} = -A_j n^2 \alpha_k \alpha_m \exp \{i n (\alpha_1 x_1 + \alpha_2 x_2 + \alpha_3 x_3 - vt)\}$$

There now exists three equations which describe the propagation of a plane wave through an orthotropic material.

These equations are written together as the product of a two dimensional matrix of elastic constants (K_{ij}) and a vector of amplitude coefficients (A_j), which is set to zero.

$$(K_{ij}) (A_j) = 0$$

This is written in an expanded form as,

$$\begin{pmatrix} [\zeta_1] & [C_{66}\alpha_1\alpha_2] & [C_{55}\alpha_1\alpha_3] \\ [C_{66}\alpha_1\alpha_2] & [\zeta_2] & [C_{44}\alpha_2\alpha_3] \\ [C_{55}\alpha_1\alpha_3] & [C_{44}\alpha_2\alpha_3] & [\zeta_3] \end{pmatrix} \begin{pmatrix} A_1 \\ A_2 \\ A_3 \end{pmatrix} = 0 \quad (15)$$

where,

$$\zeta_1 = C_{11}\alpha_1^2 + C_{66}\alpha_2^2 + C_{55}\alpha_3^2 - \rho v^2$$

$$\zeta_2 = C_{66}\alpha_1^2 + C_{22}\alpha_2^2 + C_{44}\alpha_3^2 - \rho v^2$$

$$\zeta_3 = C_{55}\alpha_1^2 + C_{44}\alpha_2^2 + C_{33}\alpha_3^2 - \rho v^2$$

Equation 15 is now solved for its eigenvalues ρv^2 and eigenvectors (A_j) which correspond to solutions for velocity

T-2043

and vectors which describe particle motion. In order to solve for the eigenvalues, the determinant of the matrix K_{ij} is set equal to zero.

$$|K_{ij}| = 0$$

This matrix is real and symmetric, as such there should be three real solutions. Each of these three eigenvalues is then substituted into equation 15. For every eigenvalue there is a solution of vector A_j corresponding to an eigenvector. These eigenvectors correspond to the direction of particle motion and are mutually orthogonal.

There are now three solutions, each consisting of an eigenvalue and an eigenvector. The three eigenvalues are generally unequal, and correspond to the velocity of propagation. For any arbitrary direction of propagation, the three solutions were labelled on the basis that the velocity should be a continuous function of direction. One of the three solutions (labelled longitudinal) is a high velocity phase with a particle motion almost parallel to the direction of propagation. The other two solutions

(labeled t_1 and t_2) have slower velocities (generally unequal), with particle motion in a plane almost normal to the direction of propagation.

In order to facilitate the visualization of the particle motion a new set of cartesian axes was devised. In Figure 8 the new system axes (L , T_h , T_v) are rotated relative to the x , y and z axes, first by an amount θ around the z -axis in the y direction, then in a clockwise direction about the T_h axis by an amount $(90 - \theta)$.

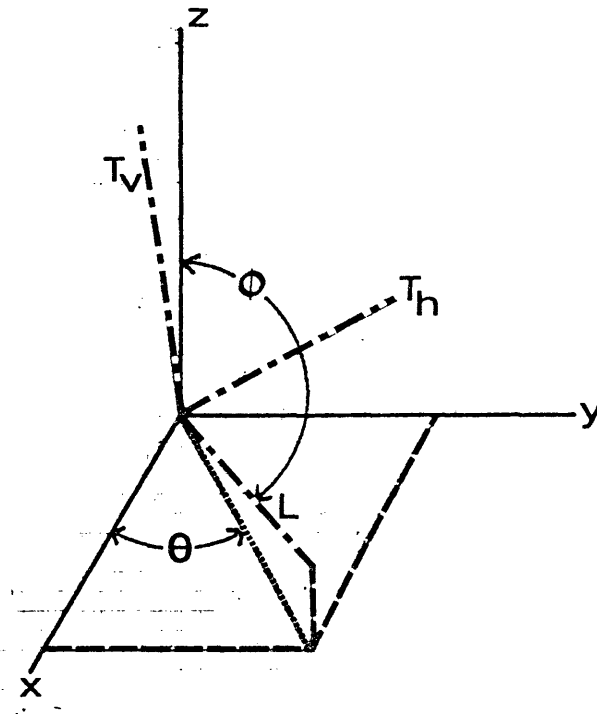


Figure 8
Geometry of propagation

T-2043

This leaves the T_h axis in the x-y plane. Only the positive axes are shown in the figure. The L axis (longitudinal) is also the direction of propagation, the T_v axis (transverse-vertical) and T_h axis (transverse-horizontal) are in a plane normal to the direction of propagation. From a seismological point of view the L axis is the P-wave axis with T_v being the SV and T_h the SH axes. The amplitude of the vibration on these three axes clearly illustrates the effect of elastic anisotropy on the particle motion.

RESULTS

In the previous section, relations describing the velocity and particle motion of a plane wave were found. This section is a presentation of the results of these relations. The results are presented, but an interpretation of them is left to the following section. A primary aim here is to obtain a good understanding of what was found so the meaning of these findings can be discussed and interpreted later.

The results were obtained from a model consisting of a simple cubic packing of cuboids with an arbitrary cap radius. The details of this arbitrary model can be studied and extended to models of other cap radii. The material properties of the cuboid particles were arbitrarily assumed to be those of quartz:

$$\text{Density} = 2.65 \text{ (grams/cc)}$$

$$\text{Young's Modulus} = 10^{12} \text{ (dynes/cm}^2\text{)}$$

$$\text{Poisson's Ratio} = 0.15$$

The cap radius A is measured in units of r (one-half the

T-2043

length of the cube edge. This model uses a cap radius of $10r$. A simple cubic packing of these cuboids has an undeformed porosity of 8.54% and a bulk density of 2.42 (grams/cc). These values do not change greatly when subjected to deformation.

Two stress configurations are used, in Case I the three axial stresses (σ_x , σ_y , σ_z) are equal and have a magnitude of 11.9 bars. In Case II the axial stresses are unequal, with those in the x and y directions being 20% less than that in the z direction ($\sigma_x = \sigma_y = 9.52$ bars and $\sigma_z = 11.9$ bars). In all the figures, velocity is shown relative to the compressional velocity along the z axis. This stress anisotropy is reflected in the values of the axial elastic constants. Compressional elastic constants, it is recalled, are only affected by changes in stress in the direction of the elastic constant. The difference between two axial compressional elastic constants will be equal to the cube root of the ratio of the stresses. When considering the shear elastic constants for anisotropic axial stresses, two stresses must be considered. For example, the C_{44} elastic constant is

T-2043

associated with shear waves traveling along the y axis with vibration only in the z direction or waves propagating in the z direction with particle motion parallel to the y axis. It is for this reason that the C_{44} elastic constant is associated with the x axis. In the derivation of these shear constants it can be seen that stresses oriented parallel to the direction of propagation or the particle motion will affect the magnitude of the constant.

Particle motion is illustrated by the vibration amplitude components on the L, T_h , T_v axes. Values of these components range from zero to one. The orientation of these axes was discussed earlier and is shown in Figure 8. The three axes form a right-handed coordinate system with the L axis being in the direction of propagation, T_h is transverse and in the x-y plane (horizontal), and T_v is transverse and in the L-z plane (vertical). The amplitude components of the particle motion may be positive or negative and the sign is noted adjacent to the curves.

In each graph the angle ϕ is variable (angle from the z-axis to the direction of propagation) and θ is

T-2043

constant (angle from x axis in x-y plane). Realizing this, the figures become cross sections at values of constant θ . Velocity curves are labeled P, t1, t2, because the P solution is seen to be predominantly longitudinal with the other two solutions being transverse.

It should be remembered that these results are the solution of the wave equation with the cuboid model being used only as a means of calculating elastic constants. Labeling of the two shear modes is intended to avoid confusion with the seismological conventions of SH and SV.

T-2043

$$\text{CASE I: } \underline{\sigma_x = \sigma_y = \sigma_z = 11.9 \text{ BARS}}$$

Figures 9 - 13 show the spatial variation of velocity and particle motion for this case. In Figure 9 (a-d) only the velocity is shown, at four values of θ . The curve labeled P has predominantly longitudinal particle motion. Solutions labeled t1 and t2 correspond to the two transverse solutions. The longitudinal velocity in general decreases at all values of θ for increasing ϕ . It might initially be expected that minimal values would occur at $\phi = 45^\circ$, but this is not always the case. A minimum is found at $\theta = 0$, $\phi = 45^\circ$ and this minimum occurs at higher values of ϕ for increasing θ .

In the solutions for the transverse phases (t1, t2) the magnitude of the velocity is seen to increase, with ϕ up to $\phi = 45^\circ$. The velocity of t2 seems to be greater than t1 everywhere except at $\theta = 45^\circ$. The reasons for this change will be discussed later (see Discussion).

The particle motions for various directions of propagation are shown in Figures 10 - 13. Also included in these figures is the curve for velocity which is provided

T-2043

as a reference. In each figure there are three graphs each of which corresponds to a different solution of the wave equation (labeled longitudinal, t1, t2). The left axis ($\theta = 0$) of each graph is labeled from zero to one, both the amplitude component and velocity curves are read off it.

For the most part the three solutions correspond very well to the conventional P, SH and SV modes of propagation. The particle motion shows some important differences from these notations. At both $\theta = 0^\circ$ and $\theta = 45^\circ$ the longitudinal and t2 solutions show components of particle motion different than that expected. In the longitudinal solution (Figures 10 and 13) there is a small component of transverse motion in addition to the predominantly longitudinal motion. Note also the change in sign of the T_v component.

The t2 curves mirror the longitudinal solution. The t1 solution in both figures is seen to be completely transverse horizontal with no longitudinal or vertical components. Figures 11 and 12 ($\theta = 15^\circ, 30^\circ$) show some surprising features. In these figures the shear modes appear to change their primary direction of vibration

T-2043

as the direction of propagation changes. Between $\varnothing = 50^\circ$ and $\varnothing = 80^\circ$ the major components of vibration change as if the polarization directions were being rotated about the direction of propagation with increasing \varnothing . Notice that the t2 solution has a larger longitudinal component than the t1 solution. The point of changeover in dominant component occurs at a lower value of \varnothing at $\theta = 30^\circ$ than at $\theta = 15^\circ$.

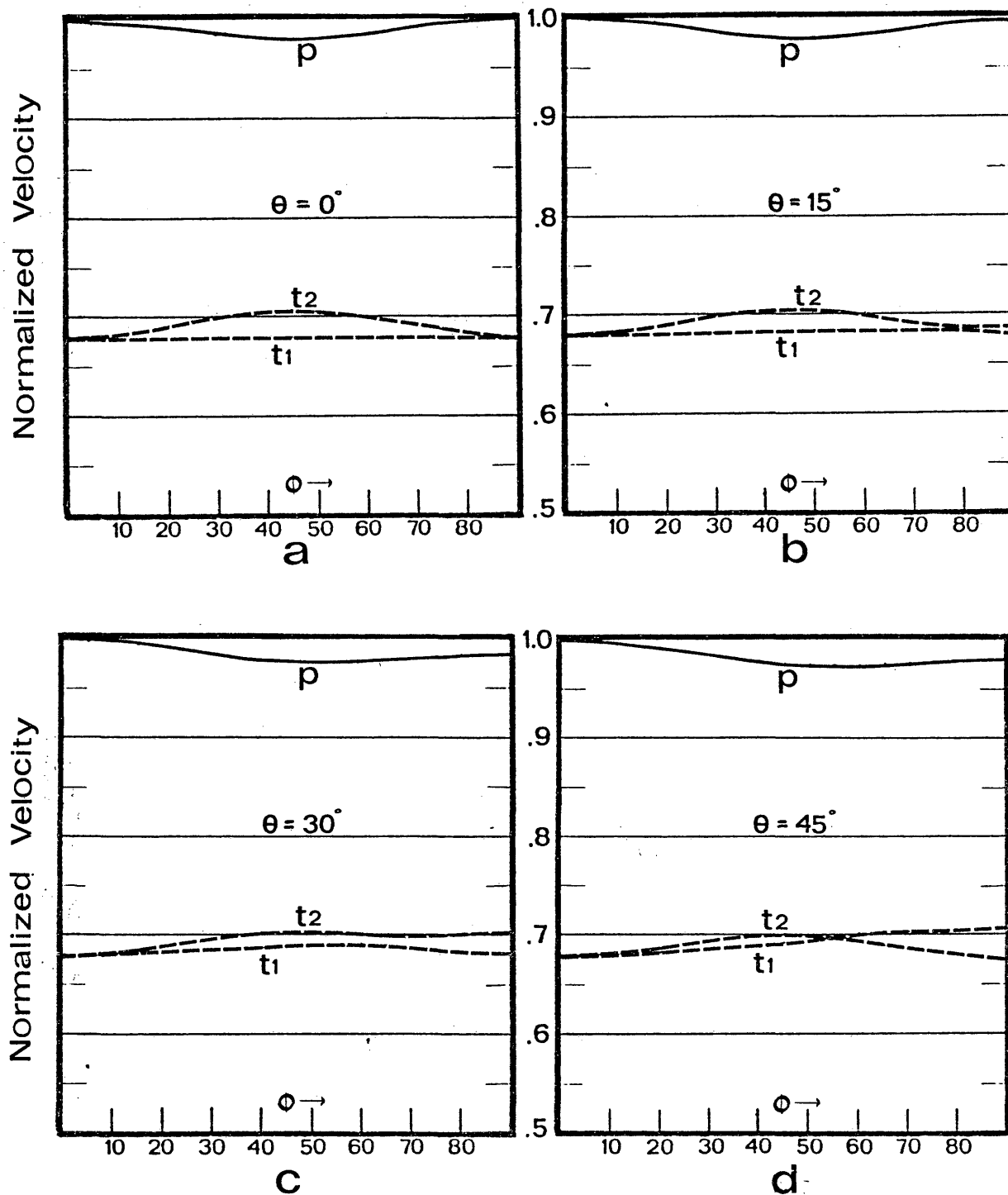
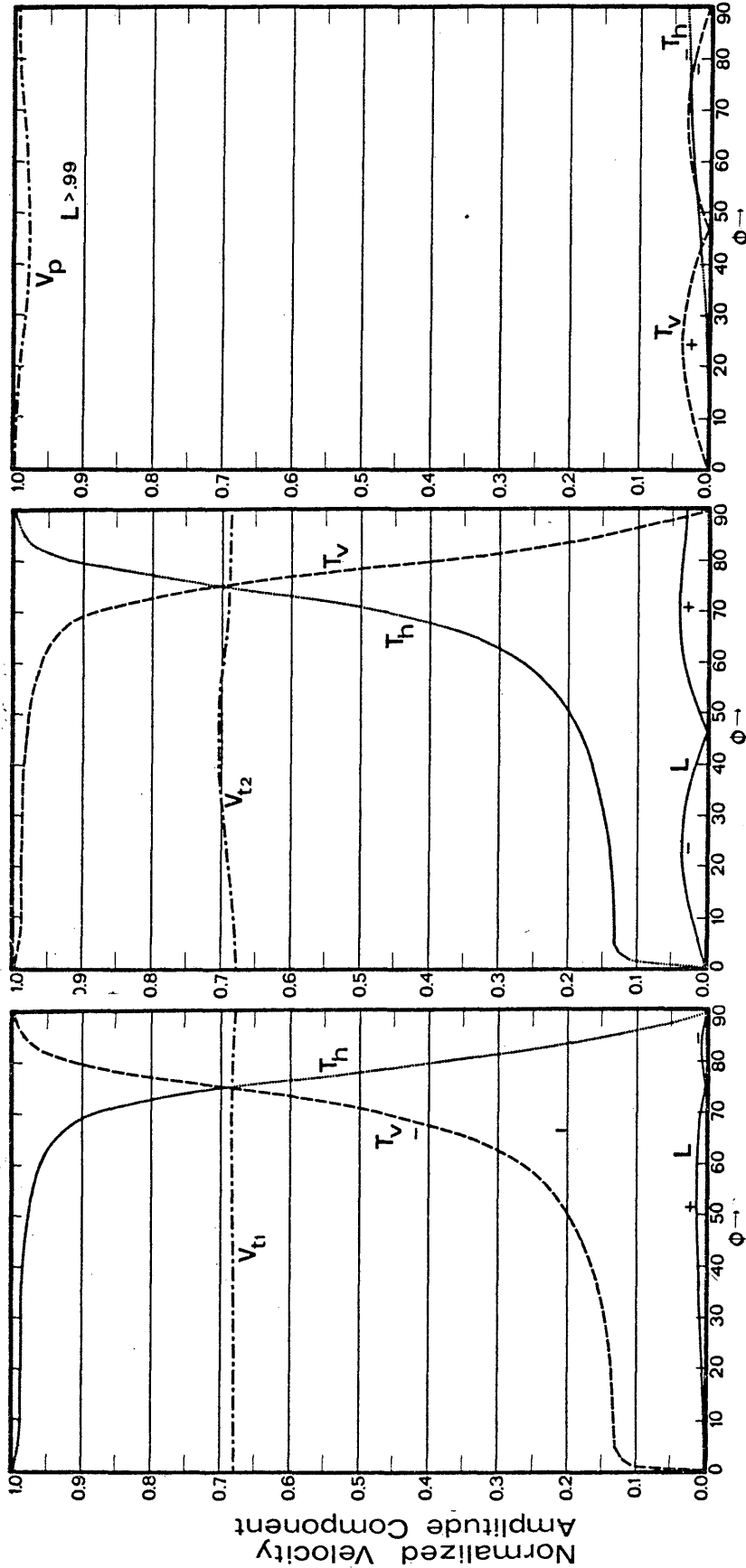


Figure 9

Dependence of relative velocities on direction in planes of constant θ . Unity is the axial velocity for the compressional wave. Stress in all axial directions is the same.



t1 solution

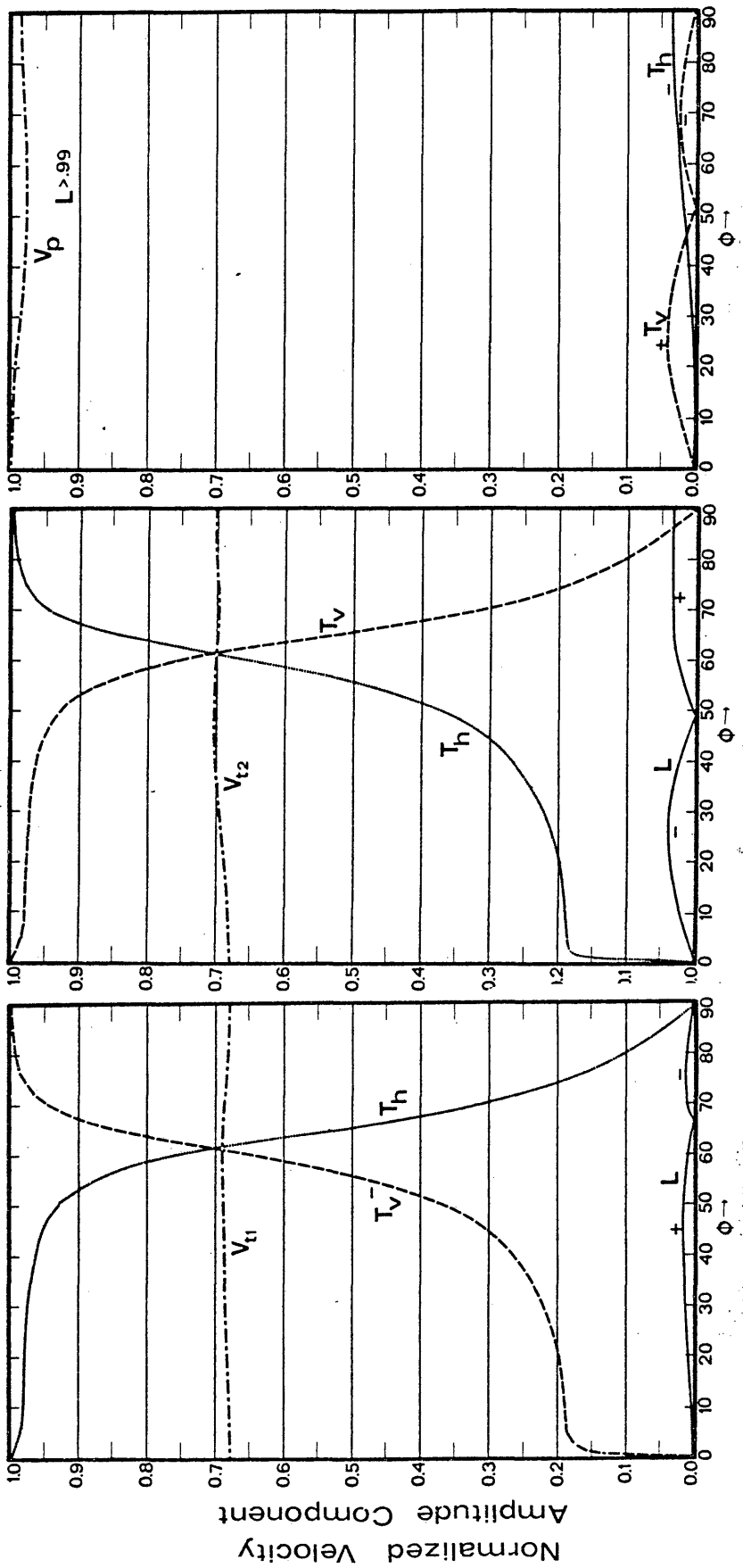
t2 solution

longitudinal solution

Figure 11

$\theta = 15^\circ$

Particle motion and velocity for a plane wave in an anisotropic medium. Individual graphs (t1, t2, and long.) illustrate separate solutions to the wave equation. The axial stresses are equal. Some component curves are labelled + or -; this indicates the sign of the value to be taken from that part of the curve. Curves not labelled + or - are assumed to be +.



t1 solution

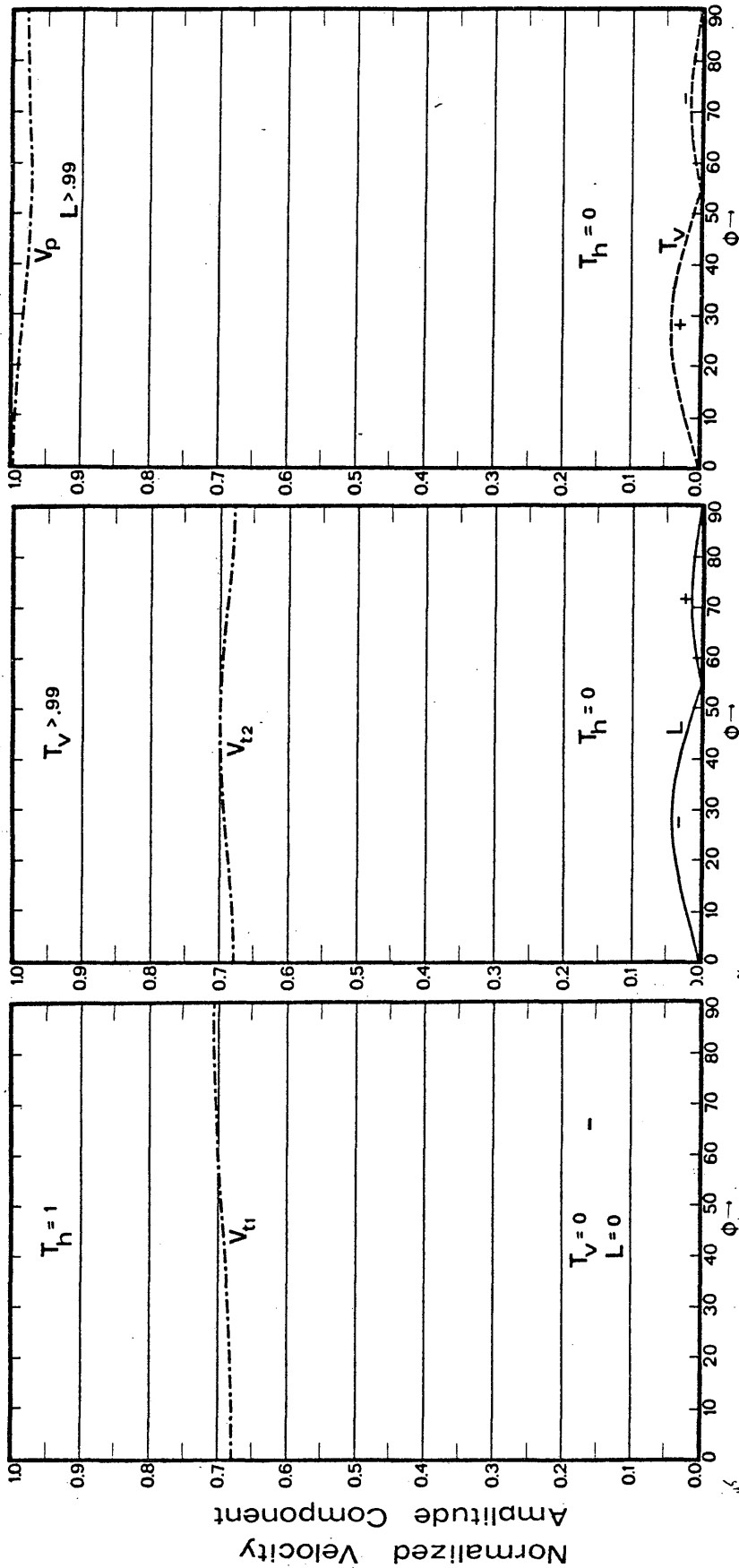
t2 solution

longitudinal solution

Figure 12

$\theta = 30^\circ$

Particle motion and velocity for a plane wave in an anisotropic medium. Individual graphs (t1, t2, and long.) illustrate separate solutions to the wave equation. The axial stresses are equal. Some component curves are labelled + or -; this indicates the sign of the value to be taken from that part of the curve. Curves not labelled + or - are assumed to be +.



t1 solution

t2 solution

longitudinal solution

Figure 13
 $\theta = 45^\circ$

Particle motion and velocity for a plane wave in an anisotropic medium. Individual graphs (t1, t2, and long.) illustrate separate solutions to the wave equation. The axial stresses are equal. Some component curves are labelled + or -; this indicates the sign of the value to be taken from that part of the curve. Curves not labelled + or - are assumed to be +.

T-2043

CASE II: $\sigma_x = \sigma_y = 9.52$ BARS, $\sigma_z = 11.9$ BARS

In this case many of the symmetries that were apparent in Case I are no longer present. Figures 14 - 18 are in exactly the same format as Figures 9 - 13. The curves themselves are of the same general shape with the primary differences being the position and magnitude of the maxima and minima.

A comparison between the velocity curves (Figures 9 and 14) show only small differences. Although these differences are small, they are caused by the stress-induced anisotropy, and are the result of different axial stresses.

The particle motion curves show some marked differences from Case I. At $\theta = 0$ the symmetry in the t_2 and longitudinal solutions is no longer apparent. In the figure for $\theta = 45$ the t_1 solution is no longer purely T_h motion. At $\theta = 15$ the dominant component of particle motion is the same at all values of ϕ where previously there was a change (or rotation) in the dominant component. The figure for $\theta = 30^\circ$ shows the rotation but the point of change in dominance is found at a higher value of ϕ than

T-2043

in Case I. At all values of θ the t_2 solution always has a greater L component than the t_1 solution. The major difference between Case I and Case II seems to be in the spatial behavior of the particle motion.

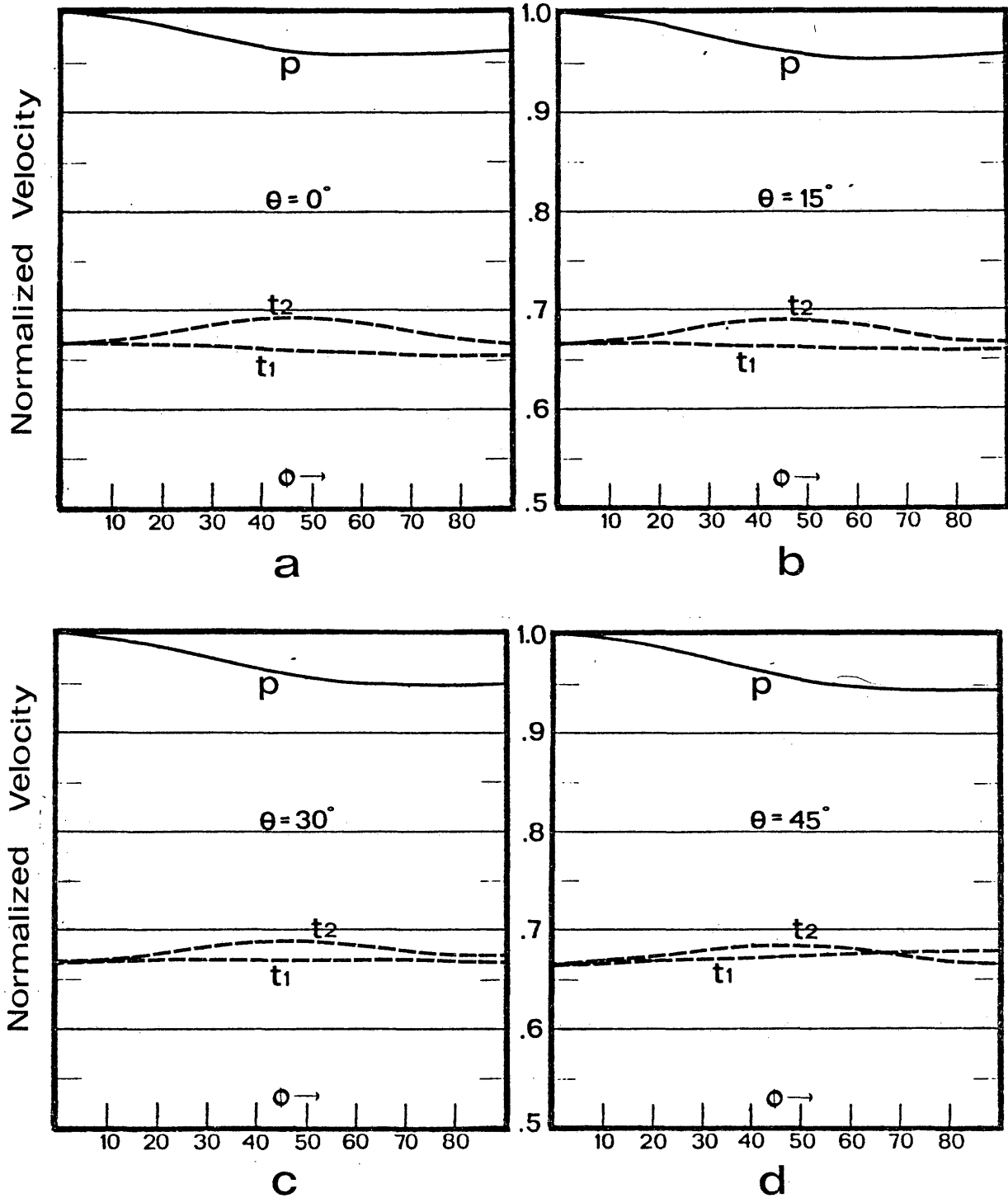
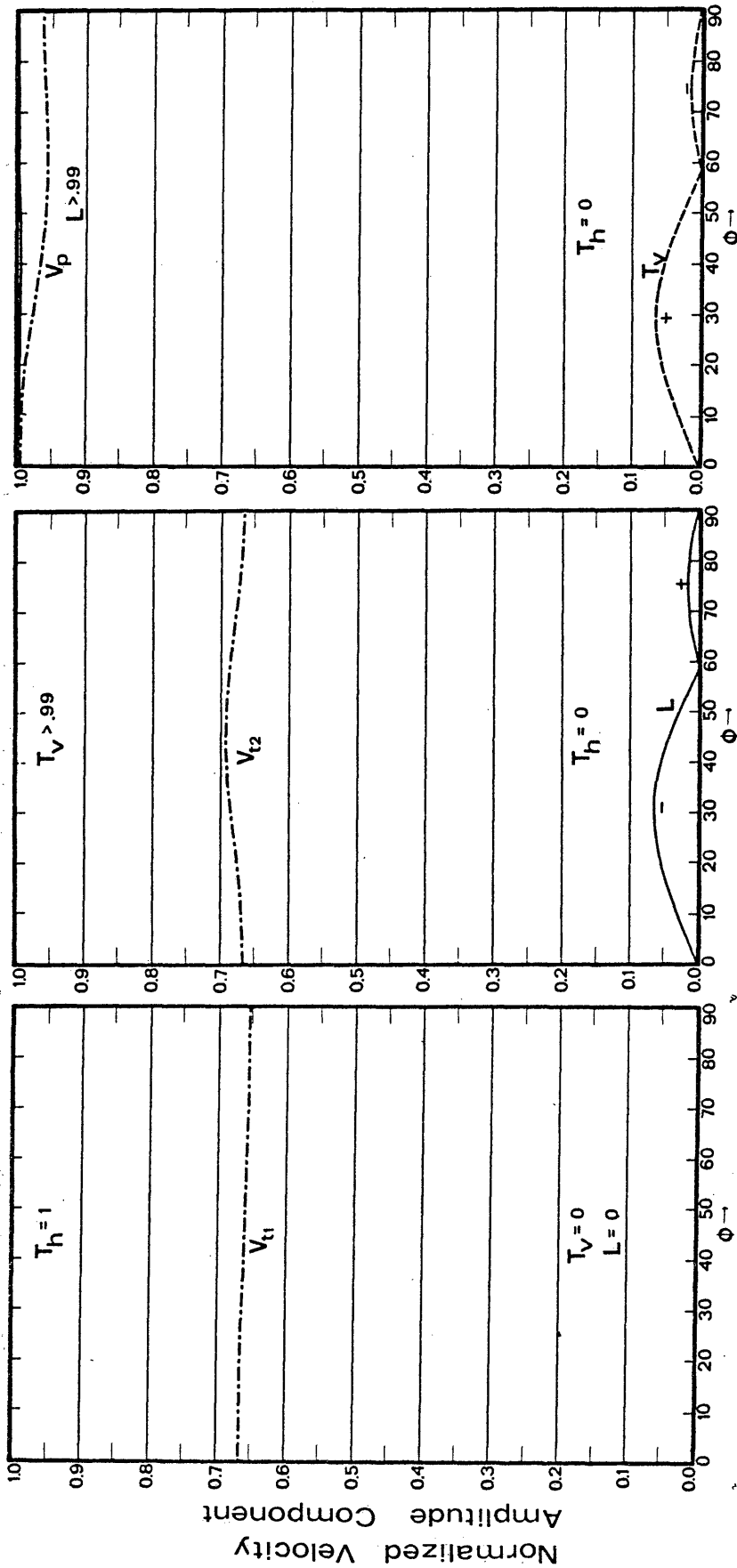


Figure 14

Dependence of relative velocities on direction in planes of constant θ . Unity is the compressional wave velocity in the z-direction. Stress in the z-direction is 20% greater than in the x and y directions.



t1 solution

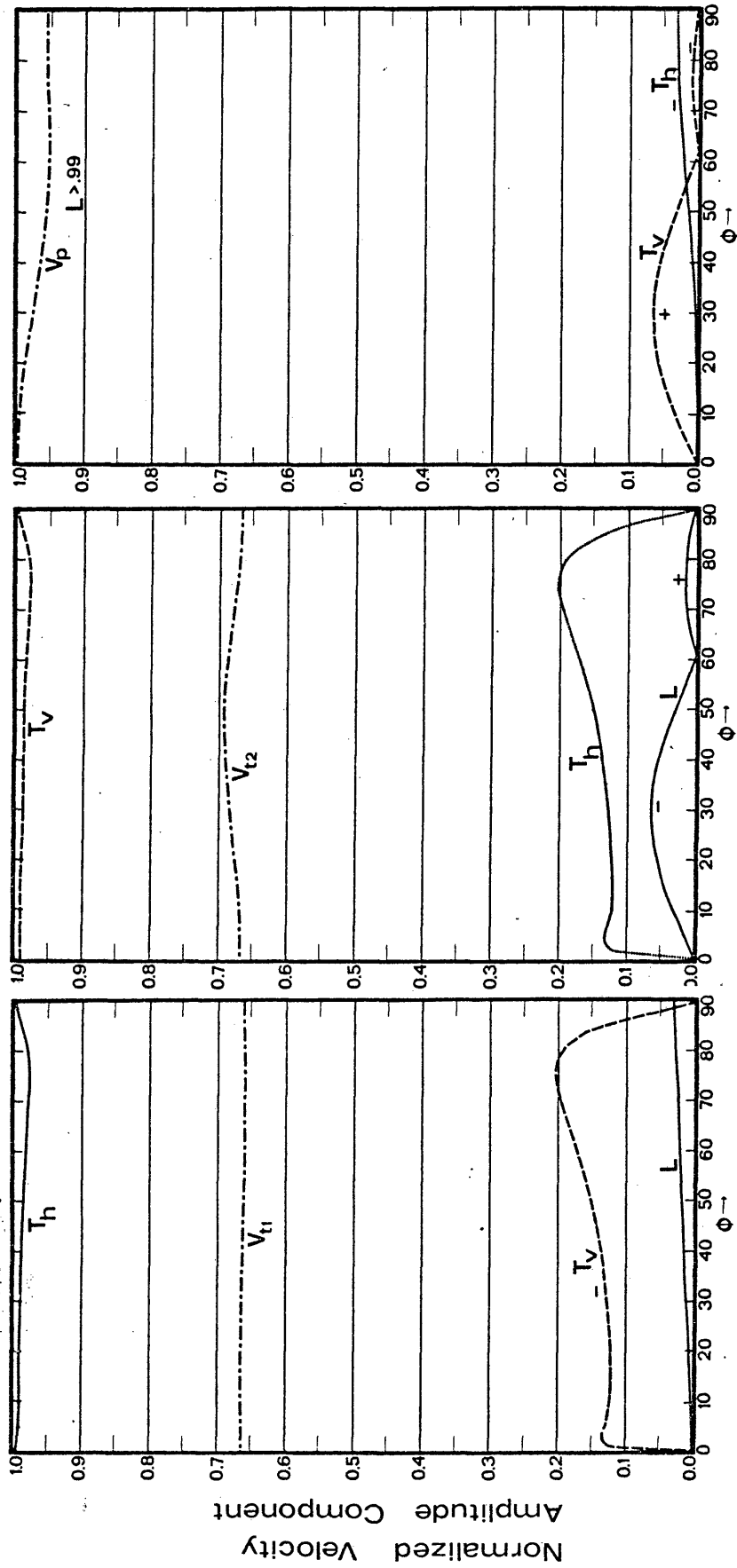
t2 solution

longitudinal solution

Figure 15

$$\theta = 0^\circ$$

Particle motion and velocity for a plane wave in an anisotropic medium. Individual graphs (t1, t2, and long.) illustrate separate solutions to the wave equation. The axial stresses are unequal. Some component curves are labelled + or -; this indicates the sign of the value to be taken from that part of the curve. Curves not labelled + or - are assumed to be +.



t1 solution

t2 solution

longitudinal solution

Figure 16

$\theta = 15^\circ$

Particle motion and velocity for a plane wave in an anisotropic medium. Individual graphs (t1, t2, and long.) illustrate separate solutions to the wave equation. The axial stresses are unequal. Some component curves are labelled + or -; this indicates the sign of the value to be taken from that part of the curve. Curves not labelled + or - are assumed to be +.

DISCUSSION

The primary aim of this section is synthesizing the insights and observations to form a good basis for drawing some conclusions. The results are examined in some detail and repeated references are made to Figures 9 - 18 of the Results Section.

Spatial Variation of Velocity

The examination of Figures 9 and 14 summarizes the spatial variation of velocity (both longitudinal and transverse). The longitudinal velocity is seen to have a greater value in an axial direction than off the axis. Even in the case where one axial velocity is less than the other, there are intermediate directions which are less than either. This minimal value occurs between 45 and 60 degrees from the direction of highest velocity. In either case the greatest change in velocity seen was about 5%.

Azimuth seems to have about the same effect on the transverse modes as the longitudinal modes. Although

T-2043

velocities are seen to change with azimuth, the magnitude of this change is on the order of 5%. The t_2 solution has a generally greater change than the t_1 and is larger in magnitude (except in one case). If the axial stresses are equal (Case I), the two solutions will be equal for propagation along any axis. In the case of unequal stresses (Case II) it should be expected that propagation in the direction of highest stress will have both shear modes of equal velocity. Both of the other two axial directions will yield two different shear velocities. It was seen earlier, in the derivation of the shear constant, that the value of the shear constant is dependent on the stress in the direction of propagation and stress parallel to the particle motion. With this knowledge the orientations of the maximum, intermediate and minimum elastic constants can be deduced. Further, if it is assumed that the medium is initially elastically isotropic, then the three directions define the orientation of the principal stresses.

The relative magnitude of the shear and compressional elastic constants plays a very important role in the spatial variation of the velocity. For most real world materials

T-2043

velocity ratios (V_s/V_p) are on the order of .6 to .7. The axial velocity ratio for this particular model is .68. For ratios which are smaller, the model shows a larger change in the magnitudes of the velocities. For example, in the previous results the choice of the model parameters resulted in an axial velocity ratio of approximately .68 and the magnitude of the variation was on the order of 5%. If model parameters were chosen such that the axial velocity ratio was about .61, the spatial velocity variation would be as shown in Figure 19. The curves in this figure can be seen to have the same basic shape as Figures 9 and 14, but the changes in velocity are now about 10%. It is readily apparent that a model with a lower velocity ratio would have a greater spatial variation and hence there would be a better chance of finding the directions of principal stress.

Spatial Variation of Particle Motion

The particle motion seems to be more sensitive to different axial elastic constants than to the difference between shear and compressional elastic constants along

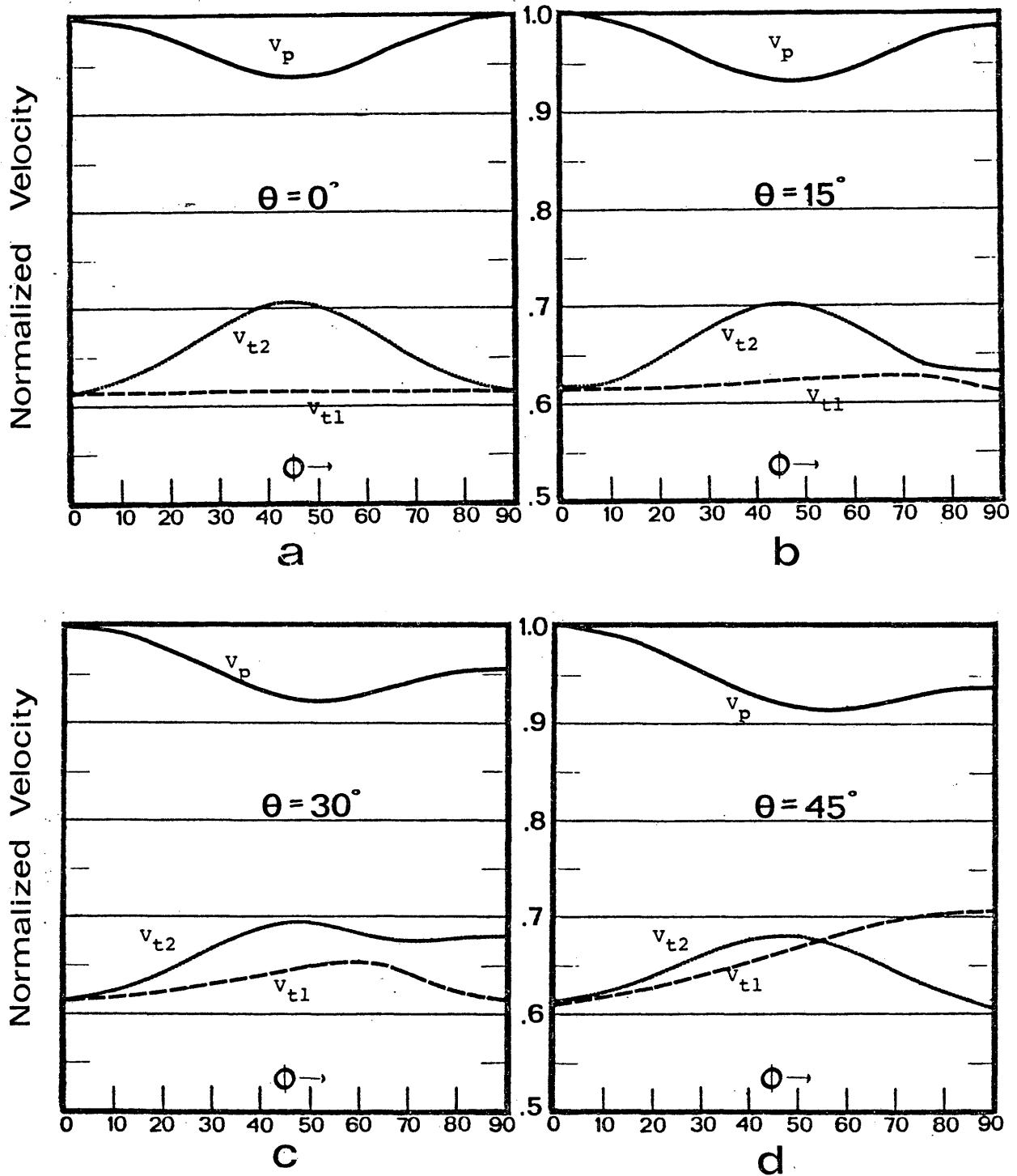


Figure 19
 Dependence of relative velocities on direction in planes of constant θ . The ratio of elastic constants is smaller than in the previous figures. Stress in all axial directions is the same.

T-2043

one axis. In other words the spatial variation of the particle motion is almost invariable if all the axial elastic constants are the same, regardless of the relative magnitude of the shear elastic constant. Differences are readily apparent between the case where the axial elastic constants are the same and the case where they are unequal (e.g., Case I vs. Case II).

The actual particle motion in an elastically anisotropic medium is not what "seismological intuition" indicates it should be. This experience says that three types of body waves exist: P, SH and SV and the particle motion for each is defined. P waves vibrate completely in the direction of propagation. SH waves have particle motions transverse to the direction of propagation and in a horizontal plane. Finally, SV motion is transverse to the direction of propagation and in a vertical plane. The results of this thesis indicate that this intuition is not applicable when the propagating medium is elastically anisotropic. The method of presentation is designed to present differences from the expected results (i.e., only P, SH, and SV motion).

Looking first at the longitudinal mode of propagation (i.e., Figures 10 - 13 and 15 - 18), it is apparent the only directions, where particle motion is always purely longitudinal, are the axial directions. In other directions the particle motion has other components. The vibration direction then is skewed relative to the direction of propagation (see Figure 20). This skewing of the particle motion is variable and can be as great as 5° or more.

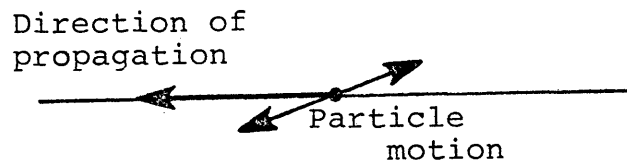


Figure 20

Particle motion of the compressional wave Propagating in an anisotropic medium.

T-2043

The direction of the particle motion when not parallel to the direction of propagation tends to be oriented in a direction which is more parallel with an axial direction of higher elastic constant. If both axial directions have the same elastic constant, the vibration tends towards the closer (in direction) axis. When both axes are equally distant, vibration is completely longitudinal. If the axes have unequal elastic constants, the particle motion tends toward the axis of greater elastic constant even though it may be more parallel to one of the other axes. The greater the difference between the axial elastic constants, the greater is the angle at which the particle motion continues to skew itself towards the axis of greatest elastic constant.

The transverse modes of vibration (solutions t_1 and t_2 , Figures 10 - 13, 15 - 18) show a markedly different spatial variation. For the axial propagation directions the vibration is polarized completely in the transverse axial directions. When propagation is in directions other than axial, the two transverse solutions are mutually perpendicular in a plane which is not quite normal to the

T-2043

propagation axis. In addition, for values of θ between 0° and 45° the two solutions rotate clockwise about a normal to their plane of vibration (direction of longitudinal vibration), as the direction of propagation changes from $\phi = 0^\circ$ to $\phi = 90^\circ$. This is not meant to say that the vibration directions of the wave rotate as it propagates. The particle motion of the wave remains constant for any direction of propagation; however, for increasing values of ϕ (constant θ) the particle motion changes in a predictable manner. In fact this changing of vibration direction is in a clockwise direction, as ϕ increases from 0° to 90° . The velocities do not show a radical change in value, in fact the t_1 solution is always less than the t_2 solution (except at $\theta = 45^\circ$). Another observation is that in the range of ϕ between 50° and 80° neither transverse solution vibrates in or near the horizontal or vertical planes.

When comparing Case I and II, it is observed that at $\theta = 15^\circ$ in Case II (Figure 16), the rotation apparent in Case I is no longer present. Instead the transverse particle motions (as ϕ increases from 0° to 90°) rotate clockwise

T-2043

a small amount (12°) and then rotate back nearly to their initial positions. In Figure 16 ($\theta = 30^\circ$) the rotation is complete, but the crossover point and the shape of the curves are more similar to those for Case I, $\theta = 15^\circ$. This suggests that for increasing values of θ , the transverse solutions show increased amounts of rotation until they reach a value at which the rotation is complete. The value of θ for which the rotation is complete appears to be dependent on the difference between the axial elastic constants. The greater the difference the larger the value of θ at which this crossover takes place.

Unlike the solutions for velocity, the spatial variation in particle motion is only affected slightly by changes in the relative magnitude of the shear and compressional elastic constants. Indeed, the particle motion seems to be a better indicator of the relative magnitude of the axial elastic constants.

Experimental Elastic Anisotropy

As was mentioned before, the results shown here are simply solutions to the homogeneous wave equation. The

T-2043

cuboid model was used only as a method of calculating elastic moduli as a function of stress. This means that the model is not necessarily one of a granular material, but of a general elastically anisotropic material with zero "Poisson's ratio". In addition, if the anisotropy is stress induced, the model becomes one which predicts the effect of the relative magnitude and orientation of the principal stresses. It is now important that these results be related to phenomena which have been or could be observed in the "real" world.

Elastically anisotropic materials have been studied in detail in connection with the idea of dilatancy and earthquake precursors. The basic idea behind these discussions (Benzing, 1973) is that most rocks, although grossly homogeneous, contain randomly oriented "penny shaped" cracks of a high aspect ratio. When these rocks, are subjected to compressional stresses, cracks oriented in or near a plane normal to the direction of stress tend to close. The closing of these cracks causes an increase in the compressional elastic constant in that direction. The increased stress also increases the shear constants

T-2043

for waves which either vibrate or propagate in the direction of the stress. The idea of dilatancy is used as a mechanism to relate changes in elastic constants to changes in stress. The model itself can only predict the effects of changes in elastic constants. In order to discuss how those constants are changed other models must be called on.

Nur and Simmons (1969) did an experimental study into stress induced velocity anisotropy in samples of Barre granite. Their results clearly show that their rock sample became anisotropic under a uniaxial stress condition. Indeed, they conclude that application of nonhydrostatic stress to a rock that contains microcracks induces elastic anisotropy. Their results for compressional waves were very similar to other experimental papers showing increases in velocity in the direction of stress and small increases in the transverse directions. The propagation of shear waves in their work seems to show some agreement with results shown in this thesis.

Figure 21 is composed of two figures from Nur and Simmons (1969). The geometry of the experimental apparatus

T-2043

is shown in Figure 21-a. A cylinder 10 cm in diameter and 10 cm long was loaded uniaxially normal to its axis, with the angle θ measured from this direction as a rotation around the axis. In Figure 21-b shows the observed waveform at the receiver for a shear wave propagating along the axis of the cylinder. The angle θ is between the direction of polarization of the transducers and the direction of applied stress. The amplitude of the waveform decreases from $\theta = 0^\circ$ to $\theta = 60^\circ$ and then increases again. Nur and Simmons attribute this change to the destructive interference of two phases propagating at slightly different velocities, vibrating in the same direction.

Using this thesis as a basis for interpretation it should be realized that the shear vibration direction for propagation along an axis of principal stress will be parallel to one or both of the other axes of principal stress. In this case the particle motion is expected to be in either the direction of applied stress or normal to it. Although the induced vibration is at an angle to the stress axis the particle motion will be skewed towards that direction. This skewing of the particle motion

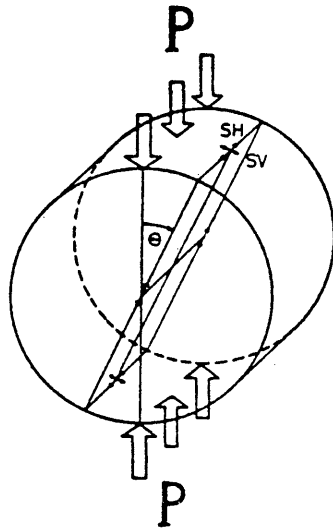
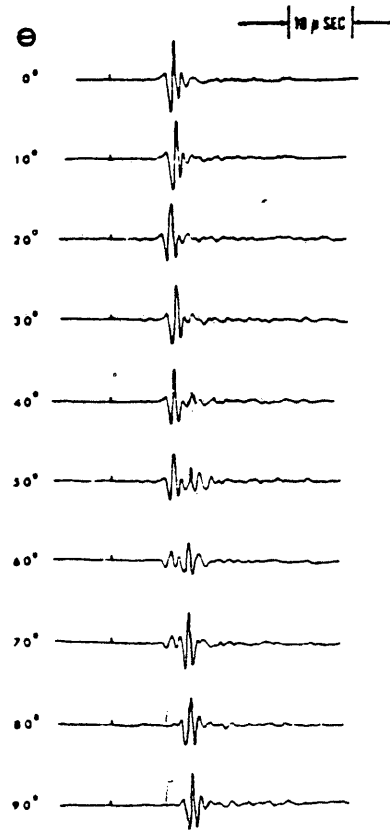


Fig. 1. Geometrical relations. The cylindrical rock sample is subjected to an applied uniaxial stress. Velocities of elastic waves are measured either along a diameter or along the axis of the cylinder. The sample, with the transducers attached, is rotated with respect to the applied stress so that the wave always travels through exactly the same path in the rock, while only the relative direction of stress is being changed. Directions of polarization of the shear transducers are indicated by *SV* and *SH*.

a



P=400 Bar
SHEAR

Fig. 7. Observed received shear wave form traveling along the axis of the cylinder at 400 bars at various angles θ between the direction of applied stress and direction of polarization of the transducers. At $\theta = 70^\circ$, the fast wave is polarized in the plane that includes the direction of the applied stress.

b

Figure 21

(a) Experimental setup and geometry. Uniaxial stress is applied in the diametral direction.

(b) Recorded wave forms for axial propagation various polarization angles θ .

(after, Nur and Simmons (1969))

T-2043

will continue until the influence of the other axis causes the particle motion to vibrate in that direction. Nur and Simmons orient their receiver parallel to the polarization of the source. According to the previous work it seems likely that the shear wave, which is propagated down the axis of the core, will not have a particle motion parallel to the induced vibration. Indeed this discrepancy will increase as the polarization angle increases; therefore, it should be expected that the amplitude of the received wave decreases as the polarization angle increases. This means that the receiver actually records a component of the actual vibration, which in the case where there is a large stress anisotropy could be much smaller than the induced amplitude.

Another point which Nur and Simmons bring up is biaxial stress. They state that there are a number of combinations of biaxial stresses which will produce the same velocity in a given direction. This ambiguity leads them to the conclusion velocity is not uniquely related to stress. They do not consider the spatial variation of velocity for each biaxial stress case nor do they consider

T-2043

shear wave velocities. In addition to these oversights, their statements are made without due consideration of the particle motion and its spatial variation. These omissions do not necessarily preclude the validity of this conclusion, but indicate that more work would have some interesting results.

CONCLUSIONS

Conventional investigations into velocity changes due to stress deal with these changes within a limited range of propagation directions. Results of these investigations indicate that in some cases changes in velocity correspond to changes in stress levels. These results do not yield an orientation or relative magnitude of the stress axes. In addition the particle motion or amplitude of the waveform seldom has been treated adequately.

In a theoretical investigation, this thesis shows that the change in velocity, between the directions of the principal stresses, can be expected to exceed 3 - 5%. The amount of this variation is found to increase from 5% when $V_s/V_p = .61$. Indeed, if the changes in stress levels cause changes in V_s/V_p , then the magnitude of variation seen will change.

The results show also that if the stress field is to be investigated, then velocity measurements of P, SH, SV type waves must be measured in a variety of directions. The relative difference in stress level in different

T-2043

directions is indicated by subtle changes in the longitudinal particle motion and large changes in the transverse particle motion. Compressional particle motion may only differ by approximately 5° , but the transverse modes actually rotate (in a clockwise direction) as propagation moves from one axial direction to another. Particle motion, if of a detectable magnitude, is a good indicator of the relative magnitude of two orthogonal stresses.

These theoretical studies indicate that the orientation and relative magnitude of the in situ stresses can be deduced from a detailed knowledge of the elastic waves. The necessary information includes velocity and particle motion for the three types of body waves (P, SH, SV). It is most important that these studies extend over a large range of azimuth and zenith.

Field investigation should take place in areas where the effects of elastic anisotropy are greatest. The spatial variation of velocity increases when the V_s/V_p ratio decreases. An examination of the spatial variation of velocity in subsurface coal mines, around a borehole, or in tectonically active areas may prove rewarding.

Earthquake seismology commonly makes use of Byerly's method of determining the orientation of the fault plane. In this method, receiver station locations are plotted on an equiangular stereonet (eg.- Wulff stereonet) according to their azimuth and extended position, relative to the earthquake epicenter. The extended position is an angular distance equal to twice the emergence angle of the compressional raypath. If the crust is sufficiently anisotropic around a particular station the particle motion will be skewed as much as 5° from the raypath. The raypath and particle motion are commonly assumed parallel, which could give rise to errors of as much as 10° in the extended position. This anisotropy may account for some of the scatter normally found on fault plane solutions.

In short, many areas of investigation are worthy of a second look in light of this work.

APPENDIX A

We can write the strain-energy potential as,

$$2W = C_{11}e_{11}^2 + C_{22}e_{22}^2 + C_{33}e_{33}^2 + 2C_{13}e_{11}e_{33} + 2C_{12}e_{11}e_{22} + 2C_{23}e_{22}e_{33} + C_{44}e_{23}^2 + C_{55}e_{31}^2 + C_{66}e_{12}^2$$

The equation of motion for a disturbance of small amplitude in a medium of density ρ is,

$$\begin{aligned} \rho \frac{\partial^2 U_1}{\partial t^2} &= \frac{\partial \Psi_{11}}{\partial x_1} + \frac{\partial \Psi_{12}}{\partial x_2} + \frac{\partial \Psi_{13}}{\partial x_3} \\ \rho \frac{\partial^2 U_2}{\partial t^2} &= \frac{\partial \Psi_{21}}{\partial x_1} + \frac{\partial \Psi_{22}}{\partial x_2} + \frac{\partial \Psi_{23}}{\partial x_3} \\ \rho \frac{\partial^2 U_3}{\partial t^2} &= \frac{\partial \Psi_{31}}{\partial x_1} + \frac{\partial \Psi_{32}}{\partial x_2} + \frac{\partial \Psi_{33}}{\partial x_3} \end{aligned} \quad (1)$$

where the stresses, $\Psi_{ij} = \frac{\partial W}{\partial e_{ij}}$

Now the stresses can be written as,

$$\begin{aligned} \Psi_{11} &= C_{11}e_{11} + C_{12}e_{22} + C_{13}e_{33} \\ \Psi_{22} &= C_{22}e_{22} + C_{12}e_{11} + C_{23}e_{33} \\ \Psi_{33} &= C_{33}e_{33} + C_{13}e_{11} + C_{23}e_{22} \\ \Psi_{12} &= \Psi_{21} = C_{66}e_{12} \\ \Psi_{13} &= \Psi_{31} = C_{55}e_{31} \\ \Psi_{23} &= \Psi_{32} = C_{44}e_{23} \end{aligned} \quad (2)$$

Neglecting body forces we can now write the equations of motion by substituting eq.1 into 2,

$$\begin{aligned} \rho \frac{\partial^2 U_1}{\partial t^2} &= \frac{\partial}{\partial x_1} [C_{11}e_{11} + C_{12}e_{22} + C_{13}e_{33}] + \\ &\quad \frac{\partial}{\partial x_2} [C_{66}e_{12}] + \frac{\partial}{\partial x_3} [C_{55}e_{31}] \end{aligned}$$

$$\rho \frac{\partial^2 U_2}{\partial t^2} = \frac{\partial}{\partial x_2} [C_{22} e_{22} + C_{12} e_{11} + C_{23} e_{33}] + \frac{\partial}{\partial x_1} [C_{66} e_{12}] + \frac{\partial}{\partial x_3} [C_{44} e_{23}]$$

$$\rho \frac{\partial^2 U_3}{\partial t^2} = \frac{\partial}{\partial x_3} [C_{33} e_{33} + C_{13} e_{11} + C_{23} e_{22}] + \frac{\partial}{\partial x_1} [C_{55} e_{31}] + \frac{\partial}{\partial x_2} [C_{44} e_{23}]$$

Now rewrite the strain in terms of the displacement U_i ,

$$\begin{aligned} \ddot{U}_1 &= C_{11} U_{1,11} + C_{12} U_{2,21} + C_{13} U_{3,31} + C_{66} [U_{1,22} + U_{2,12}] + C_{55} [U_{3,13} + U_{1,33}] \\ \ddot{U}_2 &= C_{22} U_{2,22} + C_{12} U_{1,12} + C_{23} U_{3,32} + C_{66} [U_{1,21} + U_{2,11}] + C_{44} [U_{2,33} + U_{3,23}] \\ \ddot{U}_3 &= C_{33} U_{3,33} + C_{13} U_{1,13} + C_{23} U_{2,23} + C_{55} [U_{3,11} + U_{1,31}] + C_{44} [U_{2,32} + U_{3,22}] \end{aligned} \quad (3)$$

Let the displacements be of the form,

$$U_j = A_j \exp[in(\alpha_k x_k - vt)] \quad (4)$$

where,

A_j is the amplitude in the j^{th} direction

i is the imaginary number $\sqrt{-1}$

v is the velocity in the propagation direction

n is the wave number, α_k is a direction cosine

Equation (3) can now be rewritten using eq. 4, which results in terms of two forms,

$$\ddot{U}_j = -A_j n^2 v^2 \exp[in(\alpha_k x_k - vt)]$$

and,

$$U_{j,lm} = -A_j n^2 \alpha_l \alpha_m \exp[in(\alpha_k x_k - vt)] \quad (5)$$

Using eq.5 and eq.3 and simplifying we obtain,

$$\rho A_1 v_1^2 = C_{11} A_1 \alpha_1^2 + C_{12} A_2 \alpha_2 \alpha_1 + C_{13} A_3 \alpha_1 \alpha_3 + C_{55} [A_3 \alpha_1 \alpha_3 + A_1 \alpha_3^2] + C_{66} [A_1 \alpha_2^2 + A_2 \alpha_1 \alpha_2]$$

$$\rho A_2 v_2^2 = C_{22} A_2 \alpha_2^2 + C_{12} A_1 \alpha_1 \alpha_2 + C_{23} A_3 \alpha_2 \alpha_3 + C_{66} [A_1 \alpha_1 \alpha_2 + A_2 \alpha_1^2] + C_{44} [A_2 \alpha_3^2 + A_3 \alpha_2 \alpha_3]$$

$$\rho A_3 v_3^2 = C_{33} A_3 \alpha_3^2 + C_{13} A_1 \alpha_1 \alpha_3 + C_{23} A_2 \alpha_2 \alpha_3 + C_{55} [A_3 \alpha_1^2 + A_1 \alpha_1 \alpha_3] + C_{44} [A_2 \alpha_2 \alpha_3 + A_3 \alpha_2^2]$$

By réarranging the terms and making the following substitution we can further simplify the equations,

$$\zeta_1 = C_{11}\alpha_1^2 + C_{66}\alpha_2^2 + C_{55}\alpha_3^2 - \rho v^2$$

$$\zeta_2 = C_{66}\alpha_1^2 + C_{22}\alpha_2^2 + C_{44}\alpha_3^2 - \rho v^2$$

$$\zeta_3 = C_{55}\alpha_1^2 + C_{44}\alpha_2^2 + C_{33}\alpha_3^2 - \rho v^2$$

substituting,

$$0 = \zeta_1 A_1 + [C_{12} + C_{66}]\alpha_1 \alpha_2 A_2 + [C_{13} + C_{55}]\alpha_1 \alpha_3 A_3$$

$$0 = [C_{12} + C_{66}]\alpha_1 \alpha_2 A_1 + \zeta_2 A_2 + [C_{23} + C_{44}]\alpha_2 \alpha_3 A_3 \quad (6)$$

$$0 = [C_{13} + C_{55}]\alpha_1 \alpha_3 A_1 + [C_{23} + C_{44}]\alpha_2 \alpha_3 A_2 + \zeta_3 A_3$$

In the body of the thesis it was assumed that compression in an axial direction produces no deformation on the transverse axes. Therefore,

$$C_{12} = C_{13} = C_{23} = 0 \quad (7)$$

Using eq.7 in eq.6, we can simplify and write a matrix of amplitude coefficients as,

$$K_{ij} = \begin{bmatrix} [\zeta_1] & [C_{66}\alpha_1\alpha_2] & [C_{55}\alpha_1\alpha_3] \\ [C_{66}\alpha_1\alpha_2] & [\zeta_2] & [C_{44}\alpha_2\alpha_3] \\ [C_{55}\alpha_1\alpha_3] & [C_{44}\alpha_2\alpha_3] & [\zeta_3] \end{bmatrix}$$

We can now write the matrix equation describing the propagation of an elastic plane wave in a media of rhombic symmetry,

$$\begin{pmatrix} K_{ij} \end{pmatrix} \begin{pmatrix} A_1 \\ A_2 \\ A_3 \end{pmatrix} = 0$$

This equation can now be solved for the eigenvalues and eigenvectors.

Appendix B

Derivation of the undeformed porosity of cubically packed cuboids.

Let V_{ss} equal the volume of one spherical cap of radius A , as shown in figure I.

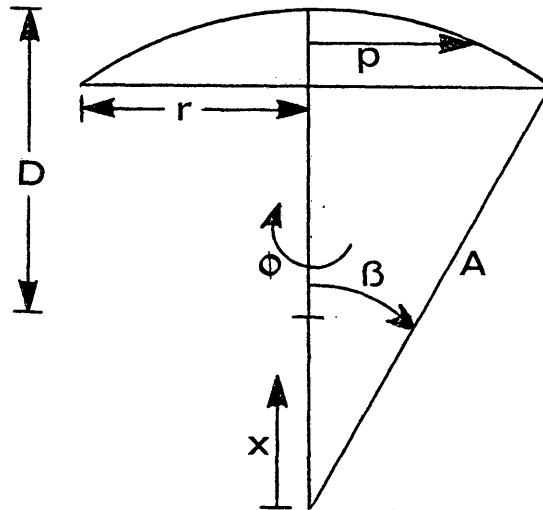


Figure I

Cuboid cap

The volume integral is set up as follows,

$$\begin{aligned}
 V_{ss} &= \int_0^{2\pi} d\phi \int_{A\cos\beta}^A dz \int_0^{(A^2-z^2)^{\frac{1}{2}}} p \, dp \\
 &= \int_0^{2\pi} d\phi \int_{A\cos\beta}^A dz \left(\frac{1}{2}(A^2-z^2) \right) \\
 &= \int_0^{2\pi} d\phi \frac{1}{2} \left[A^2 z - \frac{z^3}{3} \right]_{A\cos\beta}^A
 \end{aligned}$$

Simplifying,

$$V_{ss} = \frac{A^3}{3} \left[2 - \cos\beta(2 + \sin^2\beta) \right]$$

The total volume of the undeformed cuboid can be written as,

$$V = 6V_{ss} + V_c$$

where V_c = volume of cube = $8r^3$. Substituting the last two equations the total volume becomes,

$$V = 2 A^3 \left(2 - \cos\beta(2 + \sin^2\beta) \right) + 8r^3$$

The total volume of a unit cube containing one cuboid is,

$$V_u = D^3$$

where D is the distance between two opposite contact points and is written as,

$$D = 2(r + A(1 - \cos\beta))$$

Now, the unit volume is written as,

$$V_u = \left[2(r + A(1 - \cos\beta)) \right]^3$$

The porosity can now be written as,

$$\phi = 1 - \left(\frac{V}{V_u} \right)$$

Substituting the appropriate equations and simplifying the porosity is written as,

$$\phi = 1 - \frac{A^3(2 - \cos\beta(2 + \sin^2\beta)) + 4r^3}{4(r + A(1 - \cos\beta))^3}$$

BIBLIOGRAPHY

- Benzing, W. M., Bonner, Schock, 1973, Ultrasonic travel time in a granodiorite under uniaxial compression, Lawrence Livermore Laboratory, UCRL-51477, Livermore, California.
- Brandt, H., 1955, A study of the speed of sound in porous granular media, J. Appl. Mech., Dec. , paper no. 55, p. 479-486.
- Duffy, J., Mindlin, 1957, Stress-strain relations and vibrations of a granular medium, J. Appl. Mech., v. 24, p. 585-593.
- Gassmann, F., 1951, Elastic waves through a packing of spheres, Geophysics, v. 16, no. 4, p. 673.
- Johnson, K. L., 1955, Surface interaction between elastically loaded bodies under tangential forces, Proc. Roy. Soc., London, v. 230, p. 531-548.
- Mindlin, R. D., 1959, Compliance of elastic bodies in contact, J. Appl. Mech., v. 71, p. 259-268
- Mindlin, R. D., et. al., 1951, Effects of oscillatory tangential force on the contact surfaces of elastic spheres., Proc. First U. S. National Congr. Appl. Math, p. 203-208.
- Nur, A., G. Simmons, 1969, Stress induced velocity anisotropy in rock: an experimental study, J. Geophys. Res., v. 74, no. 27, p. 6667-6674.
- Stoneley, R., 1949, The seismological implications of anisotropy in continental structure.
- White, J. E., 1965, Seismic waves: New York, McGraw-Hill Book Company, Inc.
- _____, 1966, Static friction as a source of seismic attenuation, Geophysics, v. 31, no. 2, p. 333-339.
- White, J. E.; R. L. Sengbush, 1953, Velocity measurements in near surface formation, Geophysics, v. 18, no. 1, p. 54-69.